



In situ LA-ICPMS U-Pb dating of Sulfates: Applicability of carbonate reference materials as matrix-matched standards

Aratz Beranoaguirre^{1,2,3,4}, Iuliana Vasiliev⁵, Axel Gerdes^{2,3}

¹ Institut für Angewandte Geowissenschaften, Karlsruher Institut für Technologie, Adenauerring 20 b, 76131 Karlsruhe, Germany

² Institut für Geowissenschaften, Goethe-Universität Frankfurt, Altenhöferallee 1, 60438 Frankfurt am Main, Germany

³ Frankfurt Isotope and Element Research Center (FIERCE), Goethe-Universität Frankfurt, Frankfurt am Main, Germany

⁴ Geologia Saila, Euskal Herriko Unibertsitatea UPV/EHU, Sarriena z/g, 48940 Leioa, Spain

⁵ Senckenberg Biodiversity and Climate Research Centre (BiK-F), Senckenberganlage 25, 60325 Frankfurt am Main, Germany

10 Correspondence to: Aratz Beranoaguirre (beranoaguirre@fierce.uni-frankfurt.de)

Abstract. Recent developments on analytical capabilities in the field of in situ laser ablation mass spectrometry (LA-ICPMS) have expanded the applications of U-Pb geochronometers in low-U minerals such as carbonates or garnets. Although the rapid evolution of the technique relies on well characterized matrix-matched reference materials, the use of non-matrix-matched standards has been evaluated given the unavailability of standards for some minerals. In this article, we explore the suitability of using carbonate as reference materials for in situ U-Pb dating of sulfates. We have used the astrochronologically dated gypsum and anhydrite samples deposited during the Messinian Salinity Crisis (5.97 – 5.33 Ma) and compared these dates with the U-Pb ages obtained by LA-ICPMS. Although the majority of the samples failed due to the elevated common-Pb content and low $^{238}\text{U}/^{204}\text{Pb}$ ratios, five of the samples showed a higher dispersion on U/Pb ratios. The obtained dates in four of these samples are comparable with the expected ages while another gave an unexpected younger age, each of them with 6-11% of uncertainty. The pit depth of the spots showed that the sulfates ablate faster than carbonates, but the offset due to the crater geometry mismatch or downhole fractionation is not noticeable. To sum up, the bias between the U-Pb and expected cyclostratigraphic ages, if any, is included in the uncertainty and thus, the results obtained here suggest that carbonate reference materials are reliable for in situ U-Pb dating of sulfates.

1 Introduction

25 Latest years developments in instrumentation and analytical capabilities of LA-ICPMS techniques have widely opened the applicability of the U-Pb geochronometer. The high spatial resolution, low cost of analysis and high throughput with relatively good precision (Schaltegger et al., 2015) achievable with the new generation of laser and mass spectrometers favour the study of minerals with low and heterogeneous U concentrations like carbonates or garnets (e.g. Roberts et al., 2020). In fact, carbonate geochronology has gone from scarce publications that involve tedious and long-lasting isotope dilution techniques (e.g., Brannon et al., 1996; Grandia et al., 2000; Woodhead et al. 2006, 2012) to a bloom of dozens of publications per year (extensive review in Roberts et al., 2020). Likewise, garnet U-Pb dating is rapidly developing and skarn or metamorphic



garnets, with U contents even below 100 parts per billion (e.g., Burisch et al., 2019; Yan et al., 2020; Millonig et al., 2020). In addition, several laboratories have started to investigate the possibility of measuring other types of minerals: dolomites (Burisch et al., 2017), fluorite (Piccione et al., 2019; Lenoir et al., 2021), nacrite (Piccione et al., 2019) or anatase (Sindern et al., 2019), among others.

The rapid evolution of U-Pb dating in low-U phases is closely related to the publication and availability of reference materials (WC-1 carbonate, Roberts et al., 2017; or Mali garnet, Seaman et al., 2017). Well-characterized matrix-matched reference material is essential for U-Pb analytical techniques using ion or laser probes as it is affected by matrix effects (Sylvester, 2008; Yang et al., 2018). Indeed, LA-ICPMS dates could only be as good as the homogeneity of the reference materials, the accuracy and precision to which such material is known (Schaltegger et al., 2015). However, several authors have appraised the suitability of using non-matrix-matched standards, with different levels of success. Deng et al. (2017) and Wafforn et al. (2018) used 91500 respectively GJ1 zircon to correct U/Pb fractionation of garnet and argued that they get accurate ages, whereas Yang et al. (2018) found that the ages of garnets were 11 % older when standardizing to zircon. Similarly, Parrish et al. (2018) measured the Mud Tank zircon within carbonate analyses and they observed a bias between zircon and calcite of c. 4.7%. Due to the lack of an appropriate matrix-matched standard, Piccione et al. (2019) used the WC-1 carbonate reference material for fluorite analysis assuming that the bias between calcite and fluorite may likely be less than the one between calcite and zircon. This study aims to examine the suitability and reliability of using carbonates as reference material for dating sulfates. For such purpose, we have analysed astrochronologically dated gypsum and anhydrite samples from the Messinian Salinity Crisis (MSC) in the Mediterranean Sea (Roveri et al., 2014a, 2014b; Vasiliev et al., 2017; Grothe et al., 2020; Andreetto et al., 2021). Chronostratigraphy of Late Miocene to Early Pliocene within the MSC is well constrained (CIESM, 2008; Manzi et al., 2013, Roveri et al., 2014a) and thus, makes those samples ideal for comparison purposes. Gypsum ($\text{CaSO}_4 \cdot 2\text{H}_2\text{O}$) and Anhydrite (CaSO_4) are the two most abundant sulfates of marine and non marine evaporite deposits (e.g. Murray, 1963; Babel and Schreiber, 2014). Sedimentary gypsum forms by direct precipitation out of water evaporation under arid climatic conditions in hydrologically restricted environments. Under terrestrial evaporitic conditions, gypsum is the dominant primary mineral and anhydrite forms through gypsum dehydration caused during diagenesis. In the presence of water at shallower levels, the anhydrite is rapidly converted back to gypsum (e.g. Conley and Bundy, 1958; Murray, 1964; Ossorio et al., 2014; Warren, 2016). Although less frequent, non-evaporitic gypsum formation can also take place (see Van Driessche et al., 2019 and references therein). Accurate U-Pb dating of sulfates could contribute to a better understanding of their formation and/or transformation (hydration-dehydration) processes within different geological events.

2 Geological Background

The Messinian Salinity Crisis (MSC; 5.97-5.33 Ma) successions record extreme fluctuations in the Mediterranean's paleoceanographic and environmental conditions (e.g. Hsü et al., 1973; Krijgsman et al., 1999; Manzi et al., 2013). At the end of the Miocene, the Mediterranean's connections with the Atlantic Ocean were extremely reduced (e.g. Flecker et al., 2015;



Krijgsman et al., 2018) whereas the freshwater supply from the Eastern Paratethys increased (Flecker and Ellam, 2006; 65 Krijgsman et al., 2010). Those paleoceanographic changes lead to the formation of hypersaline water bodies and the deposition of a kilometre-thick evaporite unit (Fig. 1A) (Ryan, 2009). The original definition of the MSC referred to a marked environmental change at the base of the Tripoli diatomite formation close to the Tortonian/Messinian boundary (Selli, 1960). Astronomical tuning of the pre-evaporitic succession showed that the MSC onset was synchronous throughout the Mediterranean (e.g., Krijgsman et al., 1999; Manzi et al., 2018; Meilijson et al., 2018). According to the shallow water-deep 70 basin model (Hsü et al., 1973; Roveri et al., 2014a), evaporite precipitation was associated with a sea-level drop in the range of 1500 m, up to the almost complete desiccation of the Mediterranean; culminating in halite precipitation and marked by the incisions of deep canyons at the Mediterranean margins. In the latest years, however, a non-evaporitic gypsum formation during MSC is increasingly mentioned. Isotope analyses of gypsum hydration water and the salinity of fluid inclusions in MSC gypsum indicate large freshwater inputs during gypsum formation (Natalicchio et al., 2014; Evans et al., 2015; Costanzo et 75 al., 2019). Additionally, suggestions of the important role of sulfur-oxidizing bacteria in biogeochemically mediated gypsum formation (Grothe et al., 2020) is increasingly used to explain a low salinity, yet high concentrations of Ca^{2+} and SO_4^{2-} (cf. Clauer et al., 2000), during the formation of MSC evaporites.

According to previous publications (Roveri et al., 2008a, 2008b and 2014a), the MSC can be separated into three main stages (Fig. 1B). Stage I (5.97-5.60Ma), the so-called Primary Lower Gypsum (PLG; Lugli et al., 2010), is defined by the deposition 80 of primary selenite gypsum unit. During the stage II (5.60-5.55 Ma), large evaporite deposits occurred (Resedimented Lower Gypsum unit, RLG), which includes halite, gypsum cumulates and brecciated limestones ('Calcare di Base' type 3; Manzi et al., 2011). Likewise, clastic gypsum derived from the dismantlement of the PLG unit can be also found within this stage. Finally, alternating gypsum (mainly bottom grown selenite and cumulate) and fine- to coarse-grained terrigenous deposits form the Upper Gypsum unit (UG; stage III, 5.55-5.33 Ma). There is no outcrop where the complete section of the MSC can 85 be observed, but different segments are well exposed throughout the Mediterranean

3 Methodology

U-Pb data was acquired in situ in polished mounts and slabs using a RESOLution 193 nm ArF excimer laser (CompexPro 102) equipped with a two-volume ablation cell (Laurin Technic S155) coupled to a (I) sector field ICPMS (ElementXR, ThermoScientific) or (II) multicollector ICPMS (Neptune Plus, ThermoScientific) at FIERCE (Frankfurt Isotope & Element 90 Research Center), Goethe University Frankfurt. The method is modified after Ring and Gerdes (2016) and Burisch et al. (2017). Samples are pre-screened in order to identify sub-zones with the higher $^{238}\text{U}/^{206}\text{Pb}$ ratio before each analytical session.

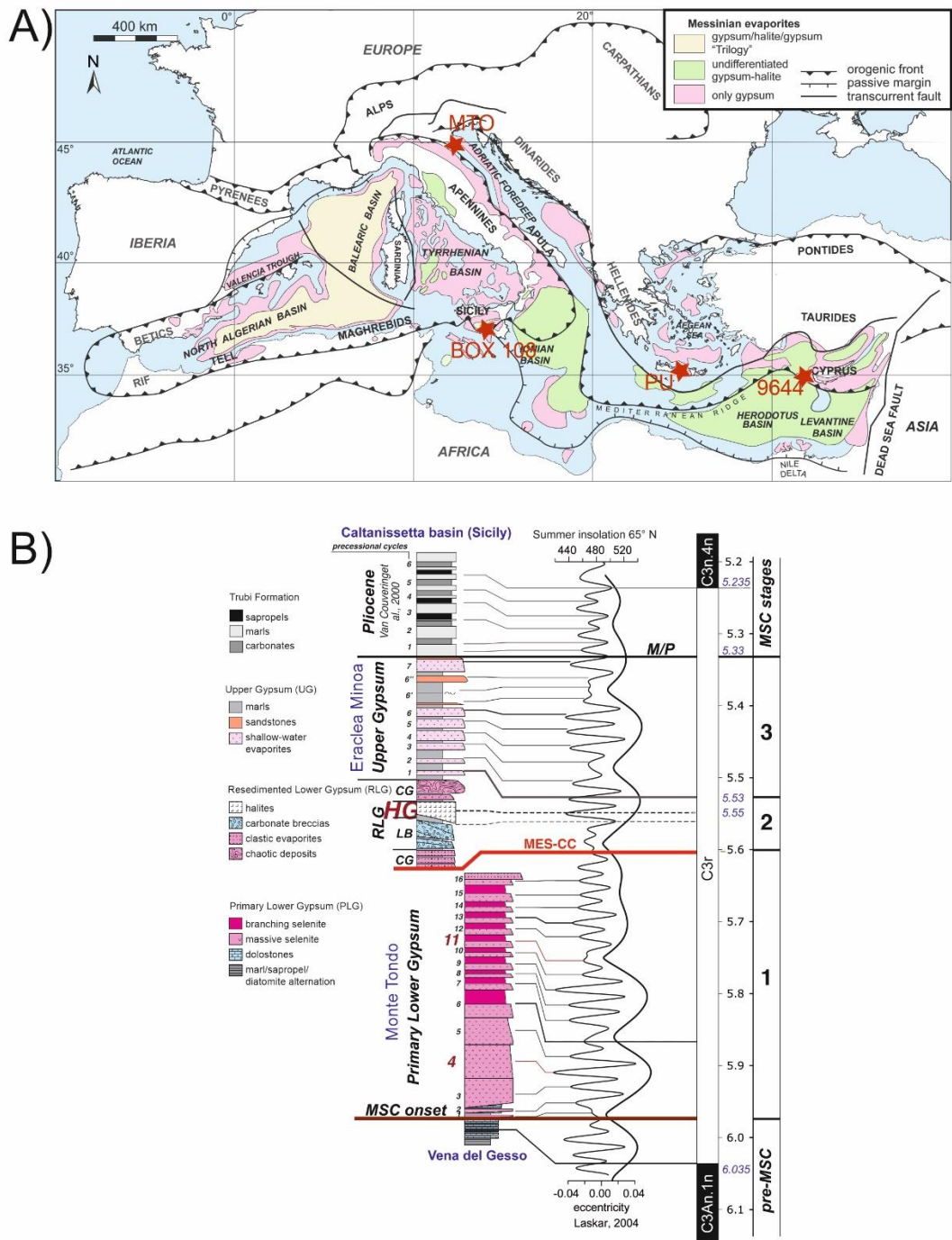


Fig. 1: A) Geological sketch of the Messinian evaporites deposits along the Mediterranean Sea (modified after Rouchy and Caruso, 2006). Note that only the successfully dated sample locations are shown. B) Chronostratigraphy of Late Miocene to Early Pliocene with MSC events in the Mediterranean (modified from Vasiliev et al., 2017).



Previous to the measurements in each of the instruments, signal strength at the ICPMS was tuned for maximum sensitivity while keeping oxide formation below $\sim 0.5\%$ (UO/U) and element fraction low (e.g. Th/U ~ 0.9). The average sensitivity for the SRMNIST614 reference material in the Element XR and Neptune Plus was ca. 700,000 cps/ppm and 6 mV/ppm for ^{238}U , respectively. In the case of the Element XR spectrometer, the detection limits (4 x background signal) for ^{206}Pb and ^{238}U were c. 0.3 and 0.03 ng/g. During 36 s data acquisition, the signal of ^{206}Pb , ^{207}Pb , ^{208}Pb , ^{232}Th and ^{238}U were detected by peak jumping in pulse counting mode. On the other hand, the detection limits in the multicollector ICPMS, were c. 0.3 and 0.5 ng/g for ^{206}Pb and ^{238}U , respectively. The analyses were done in the static multicollection mode measuring the masses ^{206}Pb and ^{207}Pb with Secondary Electron Multiplier (SEM); ^{202}Hg , ^{204}Pb , and ^{208}Pb with the Multiple Ion Counters (MIC) and ^{232}Th and ^{238}U with the Faraday cups attached to $10^{13}\ \Omega$ amplifiers. The cup intensity measured in volts is converted into cps by multiplication by a factor of 62,400. In both cases, soda-lime glass SRMNIST 614 was used as primary reference material (RM) to correct for mass bias and drift over time together with three carbonate RMs, which were bracketed in between the analysis of samples. A summary report of the U-Pb dating procedures are presented in Tables 1 and 2.

Raw data were corrected offline using an in-house VBA spreadsheet program (Gerdes and Zeh, 2006, 2009). Following background and interferences corrections, outliers ($\pm 2\sigma$) were rejected based on the time-resolved $^{207}\text{Pb}/^{206}\text{Pb}$ and $^{206}\text{Pb}/^{238}\text{U}$ ratios and the Pb and U signal. Additional matrix correction was applied to the sulfates (sector field instrument: 4.5 %; multicollector sequence 1: 8 %, sequence 2: 0.5 %, sequence 3: no offset, sequence: no offset), which was determined using WC-1 carbonate RM (254.4 ± 6.4 Ma; Roberts et al., 2017). The $^{206}\text{Pb}/^{238}\text{U}$ downhole fractionation during 16/18 s depth profiling was estimated to be 3%, based on the common Pb corrected WC-1 analyses, and was applied as an external correction to all sulfate analyses. Uncertainties for each isotopic ratio are the quadratic addition of the within run precision, counting statistic uncertainties of each isotope, and the excess of variance (Horstwood et al., 2016) calculated from the SRMNIST 614 and the WC-1 after drift correction. To account for the long-term reproducibility of the method we added by quadratic addition an expanded uncertainty of 1.5% to the final age of all analysed samples. This was deducted from repeated analyses of ASH-15D in the FIERCE laboratory between 2017 and 2019. Reference material ASH-15D (2.965 ± 0.011 Ma, Nuriel et al., 2021) and B-6 (42.99 ± 0.99 Ma; Pagel et al., 2018) were measured for quality control. In addition, an in-house RM was analysed during the first two sequences measured with the multicollector. Results on the secondary RM imply an accuracy and repeatability of the method of about 1.5 to 2%. Data were displayed in Tera-Wasserburg plots and ages were calculated as lower Concordia-curve intercepts using the same algorithms as Isoplot 4.15 (Ludwig, 2012). All uncertainties are reported at the 2σ level. After the analysis, the depth of the ablation pit was measured in several spots per sample; including the WC-1 carbonate RM, using the Keyence VHX 6000 digital microscope.



Laboratory & Sample Preparation	
Laboratory name	FIERCE, Frankfurt Isotope & Element Research Center Goethe Universität, Frankfurt am Main
Sample type/mineral	Sulphate
Sample preparation	25 mm polished resin mounts
Imaging	Petrographic microscope & 2400 dpi digital scan
Laser ablation system	
Make, Model & type	RESolution ArF excimer laser (COMpex Pro 102)
Ablation cell	Two-volume ablation cell (Laurin Technic S155)
Laser wavelength	193 nm
Pulse width	20 ns
Fluence	2 J/cm ²
Repetition rate	10 Hz
Pre-ablation	4 pulses (same parameters as main ablation)
Ablation duration	18 s
Ablation rate	~ 0.6 µm/s (in the primary RM)
Spot shape & size	Round, 154 µm (diameter)
Sampling mode	Static spot ablation
Gasses	Sample cell: He. Funnel: He + Ar. Tubbing: He + Ar + N
Gas flows	He (300 ml/min), Ar (1050 ml/min), N (8 ml/min).
ICP-MS Instrument	
Make, Model & type	ThermoScientific ElementXr sector field ICP-MS
Sample introduction	Ablation aerosol
RF power	1300 W
Detection system	Secondary electron multiplier (with conversion dynode at -8kV). Simultaneous analogue and counting (pulse) modes of detection (conversion factors calculated per mass and applied offline). Magnetic field fixed. Detection by peak jumping with electrostatic analyzer.
Masses measured	206, 207, 232, 238
Dwell times	206: 6.4 ms, 207: 7.5 ms, 232: 2.0 ms, 238: 4.6 ms
Samples per peak/integration type	4 for all masses/average
Total time per run	99 ms
Number of runs/total time	370 / 36.6 s
Acquisition mode	Trigger from laser (20 s after pre-ablation), background: 18 s, ablation: 18 s
Dead time	29 ns
Data Processing	
Gas blank	20 s on-peak zero subtracted.
Calibration strategy	NIST SRM-614 as primary RM, WC-1 as offset RM, and ASH15D as validation RM.
Reference Material (RM) information	Soda-lime glass NIST SRM-614, WC-1 (Roberts et al., 2017), ASH15D (Vaks et al., 2003)
Data processing / LIEF correction	In-house VBA spreadsheet program (Gerdes and Zeh, 2006, 2009). Intercept method for LIEF correction, assumes cPb corrected WC-1 and samples behave identically.
Mass discrimination	²⁰⁷ Pb/ ²⁰⁶ Pb (0.2%) and ²⁰⁶ Pb/ ²³⁸ U (5%) normalised to primary standard
Common-Pb correction	No common-Pb correction applied to the data.
Uncertainty level & propagation	Uncertainties are quoted at 2σ absolute and are propagated by quadratic addition of the within run precision (SD of the mean of ratios in log-ratio space), counting statistics, background, common Pb correction (if applicable) and the excess of scatter (calculated from the primary RM). In addition, an excess of variance of 1.45 % (1σ), calculated from the offset RM, was added quadratically to the ²⁰⁶ Pb/ ²³⁸ U ratios. Systematic uncertainties are reported as an expanded uncertainty, considering long term reproducibility (1.5%, 2σ) and decay constant uncertainties.
Quality control / Validation	WC-1: 254.7 ± 2.3 / 4.4 Ma (2s, MSWD = 1.00, n = 28) ASH15D: 3.004 ± 0.153 / 0.159 Ma (2s, MSWD = 0.85, n = 28) (Ages are the ²⁰⁶ Pb/ ²³⁸ U lower intercept ages of the calculated isochrons with the concordia curve in the Tera-Wasserburg space)

Table 1: LA-SF-ICPMS U-Pb analysis procedure at Goethe University Frankfurt, FIERCE laboratory.



Laboratory & Sample Preparation	
Laboratory name	FIERCE, Frankfurt Isotope & Element Research Center Goethe Universität, Frankfurt am Main
Sample type/mineral	Sulphate
Sample preparation	25 mm polished resin mounts and polished thick sections
Imaging	Petrographic microscope & 2400 dpi digital scan
Laser ablation system	
Make, Model & type	RESOLUTION ArF excimer laser (COMPex Pro 102)
Ablation cell	Two-volume ablation cell (Laurin Technic S155)
Laser wavelength	193 nm
Pulse width	20 ns
Fluence	2 J/cm ²
Repetition rate	10 Hz
Pre-ablation	2 pulses (same parameters as main ablation)
Ablation duration	16 s
Ablation rate	~ 0.6 µm/s (in the primary RM)
Spot shape & size	Round, 130 µm (75 µm for primary RM)
Sampling mode	Static spot ablation
Gasses	Sample cell: He. Funnel: He + Ar. Tubbing: He + Ar + N
Gas flows	He (300 ml/min), Ar (950 ml/min), N (ml/min).
ICP-MS Instrument	
Make, Model & type	ThermoScientific Neptune Plus multi-collector ICP-MS
Sample introduction	Ablation aerosol
RF power	1300 W
Detection system	Simultaneous multi-collection. Multiple Ion Counter (MIC) for ²⁰² Hg, ²⁰⁴ Pb, ²⁰⁶ Pb and ²⁰⁷ Pb. Faraday cups with 10 ¹³ Ω amplifiers for ²³² Th and ²³⁸ U
Masses measured	202, 204, 206, 207, 232, 238
Total time per run	131 ms
Number of runs/total time	230 / 30.1 s
Acquisition mode	Trigger from laser (14 s after pre-ablation), background: 11 s, ablation: 16 s
Data Processing	
Gas blank	11 s on-peak zero subtracted.
Calibration strategy	NIST SRM-614 as primary RM, WC-1 as offset RM, and ASH15D, B6 & in-house calcite as validation RM.
Reference Material (RM) information	Soda-lime glass NIST SRM-614, WC-1 (Roberts et al., 2017), ASH15D (Vaks et al., 2003), B-6 (Pagel et al., 2018), Calgrun (in-house calcite RM)
Data processing / LIEF correction	In-house VBA spreadsheet program (Gerdes and Zeh, 2006, 2009). Intercept method for LIEF correction, assumes cPb corrected WC-1 and samples behave identically.
Mass discrimination	²⁰⁷ Pb/ ²⁰⁶ Pb (0.2%) and ²⁰⁶ Pb/ ²³⁸ U (5%) normalised to primary standard
Common-Pb correction	No common-Pb correction applied to the data.
Uncertainty level & propagation	Uncertainties are quoted at 2σ absolute and are propagated by quadratic addition of the within run precision (SD of the mean of ratios in log-ratio space), counting statistics, background, common Pb correction (if applicable) and the excess of scatter (calculated from the primary RM). In addition, an excess of variance calculated for each sequence from the offset RM, was added quadratically to the ²⁰⁶ Pb/ ²³⁸ U ratios. Systematic uncertainties are reported as an expanded uncertainty, considering long term reproducibility (1.5%, 2σ) and decay constant uncertainties.
Quality control / Validation	Sequence 1: WC-1: 254.8 ± 1.9 / 4.3 Ma (2s, MSWD = 1.0, n = 12) B-6: 42.73 ± 0.59 / 0.87 Ma (2s, MSWD = 0.84, n = 12) CalBraun: 36.72 ± 1.23 / 1.35 Ma (2s, MSWD = 0.89, n = 12) Sequence 2: WC-1: 254.1 ± 2.0 / 4.4 Ma (2s, MSWD = 1.0, n = 20) B-6: 42.66 ± 0.47 / 0.80 Ma (2s, MSWD = 0.50, n = 22) CalBraun: 36.07 ± 0.65 / 0.85 Ma (2s, MSWD = 0.61, n = 22) Sequence 3: WC-1: 254.5 ± 3.2 / 5.0 Ma (2s, MSWD = 1.0, n = 10) ASH15D: 3.060 ± 0.193 / 0.198 Ma (2s, MSWD = 1.0, n = 10) B-6: 43.54 ± 0.79 / 1.02 Ma (2s, MSWD = 1.13, n = 10) Sequence 4: WC-1: 254.5 ± 1.6 / 4.1 Ma (2s, MSWD = 1.0, n = 20) ASH15D: 3.091 ± 0.102 / 0.112 Ma (2s, MSWD = 0.88, n = 20) B-6: 43.83 ± 0.39 / 0.77 Ma (2s, MSWD = 0.56, n = 20) (Ages are the ²⁰⁶ Pb/ ²³⁸ U lower intercept ages of the calculated isochrons with the concordia curve in the Tera-Wasserburg space. WC-1 RM are anchored at 0.85 value of ²⁰⁷ Pb/ ²⁰⁶ Pb)

Table 2: LA-MC-ICP-MS U-Pb analysis procedure at Goethe University Frankfurt, FIERCE laboratory.



4 Samples and results

4.1 U-Pb Dating

U-Pb dating was applied to 32 samples from the different locations and all available gypsum/anhydrite varieties (large selenite crystals, banded selenite, gypsum cumulates, anhydrite, halite with gypsum and anhydrite intercalation) across the Mediterranean Sea (Fig. 1), which display variable contents of Pb and U (summary in Table 3). Only five of them are successfully dated. The undatable samples are characterized by analyses that clustered near the common Pb intercept, disclosing a large amount of common-Pb (Fig. 2). This low μ ($^{238}\text{U}/^{204}\text{Pb}$ ratio) makes it impossible to draw any regression line. No link between successful/unsuccessful samples and their texture could have been established and both successful and unsuccessful samples have been found within the same type of gypsum. The successfully dated samples are described below, and their results are presented in Figs. 3 and 4 as well as in Tables 4 and 5.

Sample	U content (µg/g)	U average	Pb content (µg/g)	Pb average	n	U/Pb max
5083839	0.04-1.48	0.43	0.02-1.83	0.51	34	3.75
5083851	0.01-1.20	0.14	0.00-0.68	0.10	57	27.62
Plegio 3a	0.15-0.59	0.38	0.91-8.31	3.72	16	0.28
RB11	0.00-1.79	0.55	0.01-1.07	0.27	40	19.83
EM5 G11	0.00-0.01	0.01	0.00-0.53	0.04	16	2.22
MTO 2-3	0.00-0.59	0.24	0.00-3.53	1.10	15	0.53
MTO 3-3	0.00-0.90	0.13	0.03-1.45	0.27	43	4.89
MTO 4-4	0.02-2.34	0.97	0.00-3.85	0.31	169*	98.4
MTO 9-5	0.01-4.65	2.96	0.00-3.09	1.99	31	3.55
MTO 11-3	0.01-5.49	1.94	0.00-0.97	0.27	95*	155
MTO 14-3	0.00-1.10	0.21	0.00-0.53	0.13	15	3.58
BCR 9538	0.26-3.92	1.52	0.12-1.34	1.21	37	6.7
BCR 9539	0.00-0.58	0.18	0.00-0.58	0.15	18	11.4
BCR 9542	0.05-3.94	1.73	3.50-142.33	46.35	15	0.81
BCR 9543	0.00-19.18	6.24	0.03-140.11	29.53	78	5.00
BCR 9551	0.08-1.44	0.51	0.06-1.00	0.29	40	22.8
BCR 9552	0.00-0.58	0.09	0.77-2.43	1.27	16	0.85
BCR 9555	0.00-0.09	0.01	0.00-0.75	0.12	15	0.21
BCR 9556	0.00-0.01	0.00	0.00-0.07	0.00	15	0.92
BCR 9643	0.05-0.54	0.23	0.45-7.51	2.80	18	1.01
BCR 9644	0.01-2.31	0.33	0.00-0.61	0.03	85*	577
BCR 9645	0.00-2.63	0.37	0.02-6.86	0.77	32	18.9
BCR 9647	0.21-6.50	1.27	0.07-4.79	0.81	77*	13.3
BCR 9649	0.01-1.24	0.51	0.02-3.19	0.49	40	2.56
BOX 16	0.01-0.08	0.02	0.01-0.29	0.10	20	2.01
BOX 58	0.05-0.40	0.12	0.03-0.25	0.07	33	4.16
BOX 60	0.07-0.44	0.20	0.06-0.56	0.18	31	2.34
BOX 74	0.01-0.78	0.37	0.01-2.39	0.39	71	3.90
BOX 76	0.15-0.61	0.35	0.39-2.86	1.12	26	1.89
BOX 107	0.00-0.16	0.03	0.01-0.11	0.05	12	5.70
BOX 108	0.03-5.70	1.52	0.01-1.67	0.28	126*	158
PU05	0.00-1.44	0.20	0.00-0.16	0.01	79*	219

* sum of more than 1 day

Table 3: Compilation of U and Pb contents in all the analysed samples.

4.1.1 Sample MTO 4-4

The MTO 4-4 sample was collected at Monte Tondo gypsum quarry, located within the Vena del Gesso basin (along the western Romagna Apennines), and belongs to the PLG (Lugli et al., 2007, 2010; Vasiliev et al., 2017). It is a banded selenite (type F4 of Lugli et al., 2010) and the cyclostratigraphic age is 5.920 Ma, close to the onset of the MSC. The sample was measured in three different sequences. The maximum U and Pb content on the analysed spots are 2.34 µg/g and 3.85 µg/g, respectively; depicting a maximum U/Pb ratio of 98.4 in the best case. The first of the sequences was measured with the SF-



ICPMS and the analyses define a regression line with a lower intercept at 6.01 ± 1.19 Ma (MSWD = 1.07, Fig. 3). The other two sequences were measured with the MC-ICPMS and the lower intercept of the regression lines are 5.55 ± 0.61 Ma (MSWD = 1.00, Fig. 4) and 5.73 ± 0.37 Ma (MSWD = 1.13, Fig. 4).

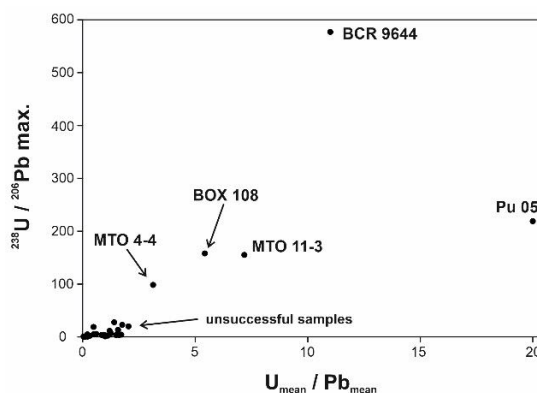


Fig. 2: Diagram showing U_{mean} content/ Pb_{mean} content vs. maximum value on $^{238}\text{U}/^{206}\text{Pb}$ axis. The successfully dated samples have a distinctively higher U/Pb heterogeneity.

4.1.2 Sample MTO 11-3

This sample was also collected by Vasiliev et al., (2017) at the Monte Tondo gypsum quarry. It is a massive selenite (F3 of Lugli et al., 2010) and belongs to the younger cycles of the PLG. Its estimated cyclostratigraphic age is 5.701 Ma. MTO 11-3 was measured as well in three different sequences. The maximum U and Pb content on the analysed spots are $5.49 \mu\text{g/g}$ and $0.97 \mu\text{g/g}$, respectively; depicting a maximum U/Pb ratio value of 155.2 in the best case. The first of the sequences was measured with the SF-ICPMS and the analyses define a regression line with a lower intercept at 5.40 ± 0.84 Ma (MSWD = 1.13, Fig. 3). The other two sequences were measured with the MC-ICPMS and the lower intercept of the regression lines are 5.46 ± 0.44 Ma (MSWD = 1.41, Fig. 4) and 5.55 ± 0.32 Ma (MSWD = 1.03, Fig. 4).

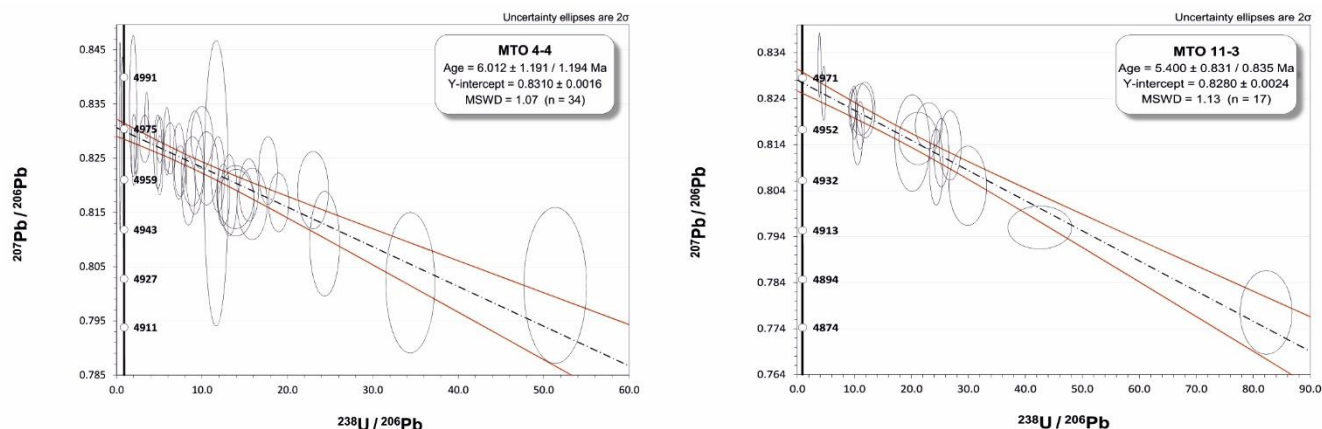
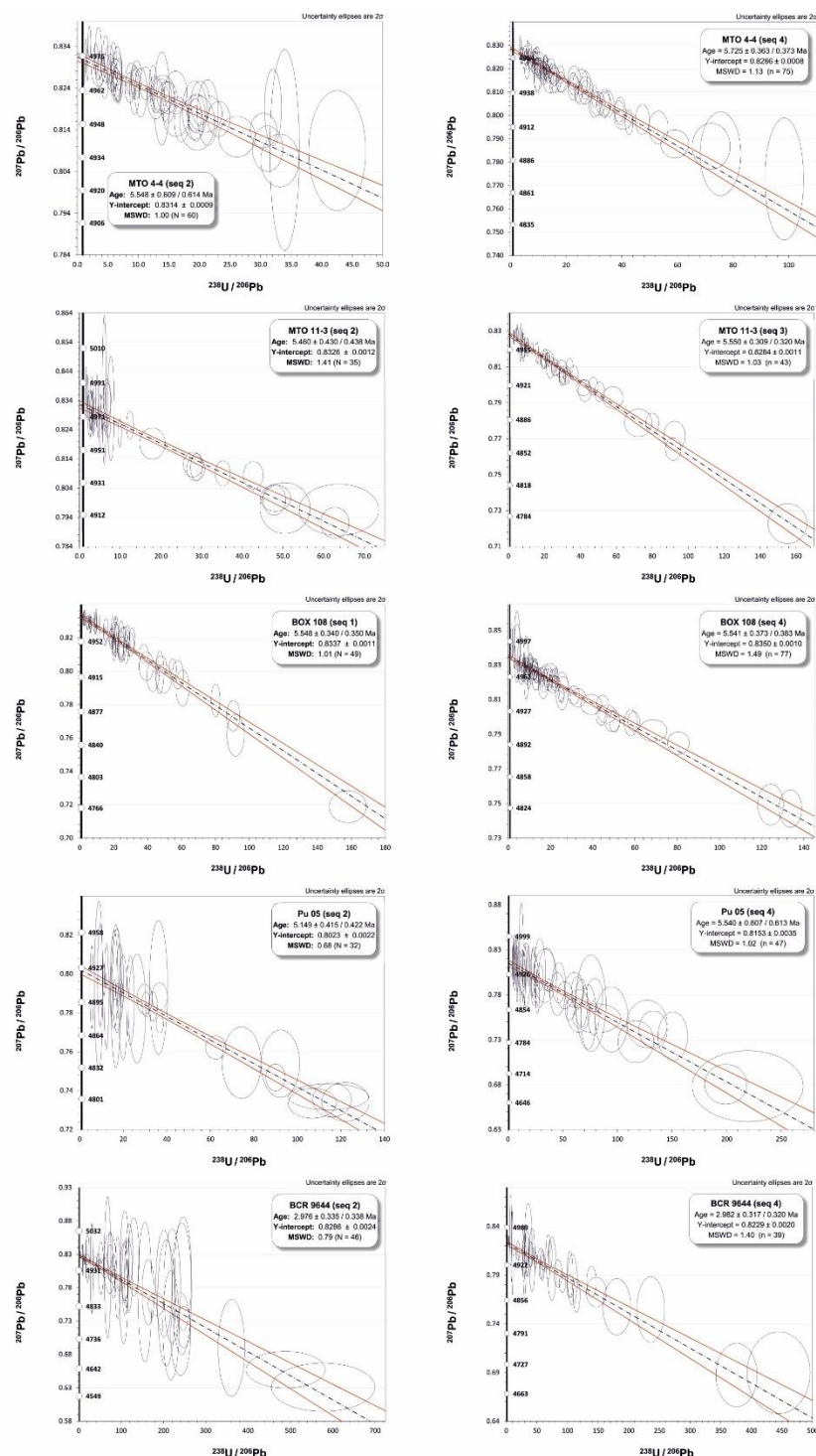


Fig. 3: Tera-Wasserburg diagram ($^{207}\text{Pb}/^{206}\text{Pb}$ vs. $^{238}\text{U}/^{206}\text{Pb}$) for the samples MTO 4-4 and MTO 11-3, measured with the sector field ICP-MS.



165 **Fig. 4: Tera-Wasserburg diagram ($^{207}\text{Pb}/^{206}\text{Pb}$ vs. $^{238}\text{U}/^{206}\text{Pb}$) for the samples MTO 4-4, MTO 11-3, BOX 108, Pu 05 and BCR 9644. All of them were measured with the multicollector ICP-MS. Each of them was measured twice in two independent sequences.**



4.1.3 Sample BOX 108

BOX 108 is a halite with anhydrite nodules. It comes from the borehole EMS-4 (Cattolica Eraclea) in the Caltanissetta Basin (southwest of Sicily) and was donated to Prof. Cita (University of Milano). The core was drilled from - 82 m to -665 m below sea water level and the sample was located almost at the bottom (approximately at - 610 m). Cyclostratigraphic ages point to 5.55-5.60 Ma. The analyses were made both in halite and in anhydrite, but only the anhydrite was successful. It was measured twice with the MC-ICPMS. The maximum U and Pb content on the analysed spots are 5.70 $\mu\text{g/g}$ and 1.67 $\mu\text{g/g}$, respectively; depicting a maximum U/Pb ratio value of 158.0 in the best case. The analyses define a regression line with a lower intercept at 5.55 ± 0.35 Ma (MSWD = 1.01, Fig. 4) in the first of the sequences and 5.54 ± 0.38 Ma (MSWD = 1.49, Fig. 4) in the second.

4.1.4 Sample BCR9644

The sample BCR9644 was collected from the cores of Deep Sea Drilling Program Site 42A hole 376 cored in 1975 West of Cyprus and stored at Bremen International Ocean Drilling Program repository. BCR9644 was collected from a Gypsum Breccia, at 170.28 m below sea level and has a stratigraphic age of ca. 5.55 - 5.60 Ma. It was measured twice with the MC-ICPMS. The maximum U and Pb content on the analysed spots are 2.31 $\mu\text{g/g}$ and 0.61 $\mu\text{g/g}$, respectively; although Pb rarely exceeds 0.1 $\mu\text{g/g}$. The maximum U/Pb ratio obtained in that sample is 577.5 in the best case. The low Pb contents imply large error ellipses, but successful regression lines have been defined, with a lower intercept at 2.98 ± 0.34 Ma (MSWD = 0.79, Fig. 4) in the first of the sequences and 2.98 ± 0.32 Ma (MSWD = 1.40, Fig. 4) in the second.

4.1.5 Sample Pu 05

This sample was collected in the Ploutis region (Central Crete, Greece) and it is a gypsum breccia. The stratigraphic age of these gypsum units is disputed between being part of the PLG (Zachariasse et al., 2008) but the texture is direct capping by Lago Mare deposits strongly suggest that Pu 05 belongs to the UG unit. Its Cyclostratigraphic age is ca. 5.40 Ma. Pu 05 was also measured twice with the MC-ICPMS. The maximum U and Pb content on the analysed spots are 1.44 $\mu\text{g/g}$ and 0.16 $\mu\text{g/g}$, respectively; depicting a maximum U/Pb ratio value of 158.0 in the best case. Each sequence define two a regression line with a lower intercept at 5.15 ± 0.42 Ma (MSWD = 0.68, Fig. 4) and 5.54 ± 0.61 Ma (MSWD = 1.02, Fig. 4), respectively.

4.2 Pit-depth measurements

After the analyses, pit-depths were measured in all the samples as well as in the carbonate reference materials. The measured pit-depth averages were used for calculating the U and Pb contents (Tables A4 and A5). The shape and depth of the craters in WC-1 primary carbonate are all similar and the average depth of them is 15.0 μm (SD = 1.34; n = 16). Few spots corresponding to the secondary reference materials were also checked and they are comparable to those of WC-1. The pit-depth of samples MTO 4-4 and MTO 11-3 is rather homogeneous with mean values of 29.6 μm (SD = 6.2; n = 44) and 18.9 μm (SD = 5.9; n =



37, Fig. 5A), respectively. The samples BCR 9644 and BOX 108 display zones with different heights in some of the ablation holes (Fig. 5B). Although they are exceptional, two ca. 90 μm and two ca. 60 μm pits were measured in BOX 108. Considering them, the average depth is 28.2 μm (SD = 16.4, n= 64) whereas excluding those four heights the standard deviation improves substantially (25.0 μm ; SD = 8.8; n = 60). The average depth for the sample BCR 9644 is 16.2 μm (SD = 6.7; n=32) excluding two ca. 60 μm spots. On the other hand, the sample PU 05 shows higher variability and larger standard deviation, since the pit-depth varies from 29 μm to 107 μm . The calculated average is 62.6 μm (SD = 23.0; n = 48).

5 Discussion

5.1. High common-Pb content

205 The majority of the analyzed samples, 27 out of 32, were unsuccessful due to the high common-Pb content and hence, low or non-existent spread in the $^{238}\text{U}/^{206}\text{Pb}$ axis. Recent studies in the field of environmental hazard have shown that Pb tends to incorporate into sulfates, both gypsum and anhydrite (Astilleros et al., 2010; Morales et al., 2014; Kameda et al., 2017). In fact, in presence of high-Pb fluids anglesite (PbSO_4) is simultaneously intergrowth with those sulfates. The behaviour of uranium remains unknown, although experiments carried out on phosphogypsum, a waste by-product generated from apatite in the production process of phosphoric acid and phosphate fertilizers, suggest that U uptake by gypsum is pH controlled (Lin et al., 2018). Thus, the more alkaline the environment is the higher U concentration could be expected in gypsum. However, the pH of evaporating seawater rarely reaches those values and tends to drop as the evaporation process goes on (Babel and Schreiber, 2014). Considering a low salinity, but high concentrations of Ca^{2+} and SO_4^{2-} (cf. Clauer et al., 2000) during the formation of MSC evaporites, the alkalinity of the depositional environment might have increased. In any case, even the gypsum precipitated in U-rich environments like uranium mine tailings contain a high amount of Pb among other metals (Liu and Hendry, 2011).

The first set of samples was measured with the sector-field single-collector ICPMS (Element XR). The U and Pb contents in the samples are rather low and produce large error ellipses in every single spot. This issue, together with low μ ratios, produces substantial uncertainties in the final ages (Fig. 3) and a comparison with the depositional ages is meaningless. In order to achieve better results, we decided to accomplish subsequent measurements with the multicollector ICPMS (Neptune Plus), which provides about three times better sensitivity and simultaneous isotope detection (Craig et al., 2018; 2020). The higher sensitivity implies smaller uncertainties in each spot and hence, more accurate and precise regression lines (i.e., ages) can be obtained. Indeed, the improvement in accuracy and precision is clearly illustrated in Figs. 3 and 4. For a similar spread in the $^{238}\text{U}/^{206}\text{Pb}$ axis, the uncertainties of ca. 15 % (MTO 11-3) or 20 % (MTO 4-4) obtained with the Element XR (Fig. 3) were reduced to 8 % (MTO 11-3, seq 2) and 11 % (MTO 4-4, seq 2) by using the Neptune Plus (Fig. 4).

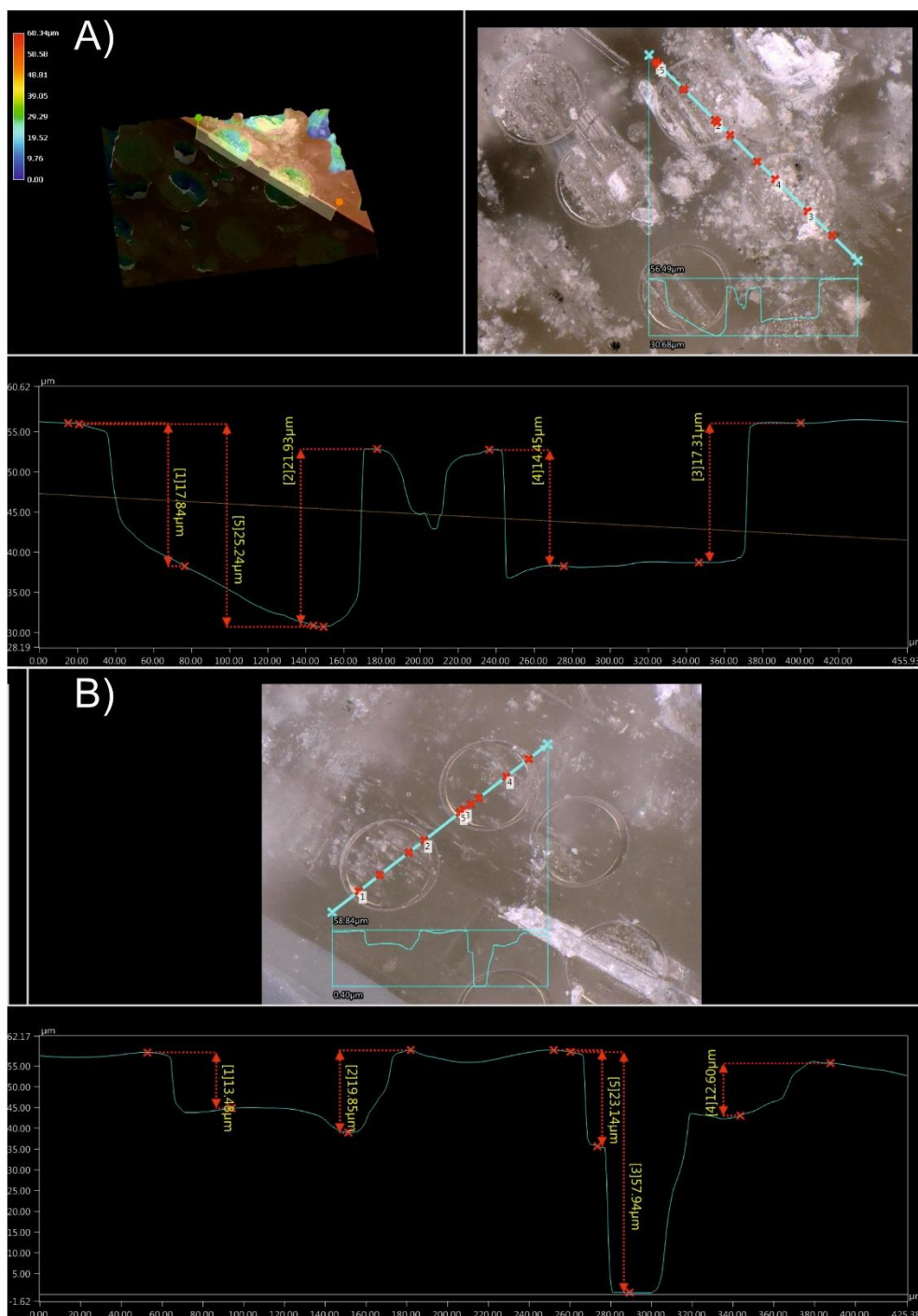


Fig. 5: Pit-depth profile of the samples MTO 11-3 (a) and BCR 9644 (b). Whereas the pit shape is roughly homogeneous in the MTO 11-3, the sample BCR 9644 displays deeper areas in some of the pits. The profiles are measured using a Keyence digital microscope VHX-6000.



5.2 U-Pb ages vs cyclostratigraphic ages

Well-characterized matrix-matched reference material is essential for U-Pb analytical techniques using laser probes as matrix differences between sample and reference standard can cause a significant offset on the obtained ages (Yang et al., 2018; Guillong et al., 2020). However, in the absence of sulfates reference materials, an attempt to use carbonate reference standards was carried out, hoping low offset between both materials. The hardness of both gypsum and calcite is similarly low and therefore, we expected that matrix-induced offset was going to be significantly lower than the one observed between carbonate and zircon (4.7 %, Parrish et al., 2018). Furthermore, both the sulfates and carbonates are easily ablated with low energy (less than 2 J/cm²), in comparison with the higher ablation energy used in some other materials, like fluorite, which needs 3 times more energy of ablation than carbonate. Nonetheless, Piccione et al. (2019) obtained analogous ages on contemporary fluorite and nacrite, both corrected to the same carbonate reference material.

The cyclostratigraphic ages of the MSC samples are known and we have used them for testing the suitability of the corrections with respect to carbonate matrix. As pointed out above, the majority of the samples contain a significant amount of common-Pb and only five ages were obtained. Although the μ of those samples was not extreme, the uncertainties range between 6 to 11 %. The ages obtained for the samples MTO 4-4, MTO 11-3, Pu 05 and BOX 108 are fully in accordance with the cyclostratigraphic ages (e.g. Lugli et al., 2007; Vasiliev et al., 2017). Unfortunately, the level of precision makes it impossible to discern whether the ages correspond to depositional or diagenetic/dehydration stages of the evaporites formation. Likewise, it is not possible to distinguish the three different stages of evaporite deposits of the MSC. Regardless, no matrix offset between sulfate and carbonate can be observed, and if any, this is included in the uncertainty.

On the other hand, the sample BCR 9644 resulted in an unexpected younger age of ca. 3 Ma. The brecciated nature of the sample, together with its extremely low Pb content (0.03 μ g/g on average) in comparison with surrounding samples (BCR9643 and BCR 9645, Table A3) suggest a subsequent (re)crystallization and remobilization of U and Pb that could be related to the breccia formation. Warthman et al. (2000) proposed an important bacterial activity after the evaporites formation. For the equivalent in time Site 374, located South-East Sicily, an ~3 m thick dolomitization front in Pliocene hemipelagic succession overlying the UG was identified. Here, an alleged role of the deep biosphere, sulfate-reducing bacteria thriving on the dissolution of sulphate bearing minerals (Warthman et al., 2000; Petrash et al., 2017) was suggested. Montano et al. (2019) showed that biological activity may control the U-Pb partitioning on carbonates, so the connection between the bacterial activity and the 3 Ma age could not be discarded. Another possible scenario could be a gypsum to anhydrite to gypsum (two-step) transformation; but there is no observation neither in the literature, that supports this hypothesis.

5.3 Pit-depth profiles

Guillong et al. (2020) showed that different ablation parameters produce distinctive pit profiles (the so-called “aspect-ratio” or depth/diameter ratio) and it could result in a noticeable bias of the data. The samples analyzed here were all ablated with the same 130 μ m spot-size, but whereas the carbonate standards result in a depth of ca. 15 μ m (aspect-ratio of 0.12) the sulfates



vary between 16 μm and 63 μm (aspect-ratio between 0.12 and 0.48, Fig. 5). This divergence between the sulfates could be devoted to various non-excluding features such as different texture, particle size, porosity or compaction (Elisha et al., 2021).
265 However, in the samples with a degree of crater geometry mismatch of less than 2 relative to the primary standard a deviation lower than 5% is anticipated (Guillong et al., 2020) which lies into the final result uncertainty. The larger aspect-ratio discordancy observed in the sample Pu 05 could result in age offsets up to 10 %. Fig. 5b reveals an important heterogeneity in the pit profile in some samples, with a silhouette that resembles pores. Whatever they correspond to porosity or chunks released due to badly coupled laser beam, nothing strange was observed in the signal.
270 These aspect-ratio and pit-depth issues are also related to the downhole fractionation corrections. Mangenot et al. (2018) claimed that shallow pit-depth compared to the spot size could minimize the downhole fractionation. That argument could apply to our reference materials and sulfates with shallower pit-depth, but how it affects depths beyond 50-60 μm can be arguable. Indeed, Lenoir et al., (2021) obtained coherent regression lines in fluorites even with pit-depths (up to 50 % variable) larger than spot sizes. Notwithstanding, the lack of bias between our U-Pb ages and cyclostratigraphic ages suggest that the
275 different downhole fractionation are not noticeable or remain within the uncertainties.

6 Conclusions

In this contribution, we have evaluated the applicability of carbonates as matrix-matched reference materials for U-Pb dating of sulfates and for that purpose, gypsum and anhydrite samples from the Messinian Salinity Crisis were analysed. The known cyclostratigraphic ages of these evaporites were compared with the in situ U-Pb ages obtained. The samples showed a high
280 amount of common-Pb and low spread in the U/Pb axis and therefore, we were forced to switch from the SF-ICPMS to MC-ICPMS in order to improve the uncertainties of the measurements. Only five samples were successfully dated. Four of them lied on the expected ages within error, while the other was considerably younger. We assume that all the factors that could produce a bias in the final age, if any, are contained in the uncertainty and therefore, the use of carbonate reference materials could be a trustworthy approach for in situ U-Pb dating of sulfates. We acknowledge that the availability of sulfate reference
285 material in the future will result in an improvement of both, reliability and precision.



Table 4: U-Pb data of the LA-SF-ICP-MS measurements.

Analysis number	name / sample	²⁰⁷ Pb ^a (cps)	U ^b (ppm)	Pb ^b (ppm)	Th ^b U	²³⁸ U/ ²⁰⁶ Pb ^c	±2σ (%)	²⁰⁷ Pb/ ²⁰⁶ Pb ^c	±2σ (%)
U436	MTO 4-4	11732	0.075	0.027	0.17	11.66	12	0.8208	3.2
U438		197284	0.26	0.46	0.32	2.043	15	0.8269	0.80
U447		1526928	0.96	3.9	0.18	0.8510	11	0.8307	0.41
U448		28825	0.034	0.066	0.33	1.942	22	0.8350	1.6
U449		25729	0.52	0.058	0.14	34.39	8.4	0.8024	1.6
U450		10535	0.34	0.024	0.11	51.35	7.2	0.8019	1.8
U451		103061	0.97	0.23	0.37	15.87	11	0.8170	0.81
U453		84862	0.67	0.19	0.11	13.91	15	0.8182	0.71
U455		813450	1.1	1.9	0.13	2.276	12	0.8266	0.50
U456		434819	0.82	0.95	0.16	3.529	6.1	0.8333	0.51
U457		334973	0.16	0.82	0.16	0.7034	21	0.8373	0.80
U458		137635	0.92	0.35	0.13	8.870	15	0.8230	0.77
U459		122106	0.41	0.25	0.14	7.284	9.8	0.8248	0.85
U460		66245	1.1	0.16	0.14	24.36	7.2	0.8096	1.2
U461		96692	1.7	0.24	0.13	23.00	7.8	0.8195	0.87
U463		153816	1.3	0.39	0.17	11.87	6.6	0.8224	0.84
U464		533967	1.5	0.96	0.15	9.984	13	0.8292	0.70
U465		198998	1.8	0.45	0.13	15.48	7.4	0.8195	0.70
U466		230504	0.82	0.58	0.22	5.050	7.3	0.8241	0.66
U467		16206	0.006	0.049	1.08	0.4013	25	0.8295	2.1
U468		392950	1.6	0.87	0.10	7.466	9.5	0.8230	0.57
U469		142184	0.56	0.34	0.18	5.895	6.3	0.8285	0.75
U470		105200	1.2	0.25	0.11	17.73	6.2	0.8231	0.76
U471		165896	1.2	0.41	0.14	10.53	13	0.8235	0.82
U472		101404	0.73	0.26	0.36	9.160	12	0.8246	1.2
U473		139917	2.0	0.35	0.11	18.97	6.2	0.8173	0.66
U474		309796	1.7	0.74	0.12	8.422	9.4	0.8193	0.76
U475		190576	2.0	0.48	0.11	14.00	15	0.8172	0.76
U476		489694	1.8	1.2	0.12	5.065	8.3	0.8288	0.51
U477		627160	1.5	1.6	0.16	3.303	19	0.8290	0.53
U479		62648	0.55	0.15	0.22	13.19	7.0	0.8186	0.91
U480		186988	0.59	0.40	0.28	6.266	11	0.8272	0.57
U481		65836	0.25	0.17	0.38	4.834	9.9	0.8266	0.82
U482		211822	1.9	0.53	0.21	12.51	6.0	0.8187	0.70
U576	MTO 11-3	62812	1.2	0.16	0.31	26.79	7.2	0.8138	0.93
U577		71210	1.6	0.18	0.21	29.91	11	0.8051	1.1
U578		27053	1.3	0.063	0.15	82.26	5.5	0.7775	1.2
U579		66175	1.1	0.16	0.33	25.25	5.2	0.8123	0.92
U580		73038	1.3	0.18	0.33	24.35	4.9	0.8092	1.0
U581		116332	0.92	0.31	0.61	9.981	5.6	0.8209	0.71
U582		183789	1.5	0.48	0.22	10.55	7.8	0.8152	0.68
U583		282627	2.0	0.73	0.30	9.601	6.3	0.8217	0.53
U584		216408	3.0	0.51	0.15	23.04	10	0.8181	0.61
U585		53627	0.56	0.12	0.34	20.15	15	0.8144	1.3
U586		93652	0.35	0.25	1.57	4.614	7.8	0.8251	0.71
U587		192319	1.5	0.47	0.24	11.90	14	0.8215	0.74
U588		350075	2.7	0.69	0.23	21.17	16	0.8154	0.70
U589		87555	0.27	0.23	2.51	3.877	6.3	0.8313	0.85
U590		298582	1.7	0.67	0.20	11.20	18	0.8216	0.68
U591		263989	3.5	0.50	0.13	42.55	13	0.7960	0.59
U592		137796	1.2	0.36	0.53	11.01	6.5	0.8182	0.63

^a Within run background-corrected mean ²⁰⁷Pb signal in cps (counts per second).

^b U and Pb concentrations and Th/U ratio were calculated relative to the primary reference material.

^c Corrected for background, within-run Pb/U fractionation (in case of ²⁰⁶Pb/²³⁸U) and



Table 5: U-Pb data of the LA-MC-ICP-MS measurements.

Analysis number	name / sample	$^{207}\text{Pb}^a$ (cps)	U^b (ppm)	Pb^b (ppm)	$\frac{\text{Th}}{\text{U}}^b$	$\frac{^{238}\text{U}^c}{^{206}\text{Pb}}$	$\pm 2s$ (%)	$\frac{^{207}\text{Pb}^c}{^{206}\text{Pb}}$	$\pm 2s$ (%)	sequence
009_U	BOX 108	47348	1.5	0.12	0.072	20.17	5.3	0.8166	0.71	1
010_U		44263	1.1	0.056	0.23	29.83	6.6	0.8160	0.89	1
011_U		8120	0.30	0.019	0.13	24.49	6.7	0.8187	1.4	1
012_U		159615	0.70	0.39	0.22	2.864	15	0.8321	0.56	1
013_U		52758	1.7	0.11	0.15	24.44	7.1	0.8109	0.68	1
015_U		45815	1.2	0.10	0.14	18.66	5.8	0.8205	0.69	1
016_U		210465	0.67	0.50	0.14	2.107	5.8	0.8319	0.50	1
017_U		153200	1.1	0.20	0.17	9.094	11	0.8307	0.56	1
020_U		8660	1.3	0.021	0.088	91.85	5.6	0.7616	1.6	1
020_Ui		54426	1.1	0.11	0.099	15.05	5.7	0.8207	0.68	1
021_U		40138	1.3	0.081	0.11	26.06	13	0.8202	0.75	1
022_U		13276	2.0	0.034	0.056	90.51	4.3	0.7733	1.2	1
024_U		15689	0.50	0.036	0.066	21.67	4.8	0.8219	1.4	1
025_U		24934	0.77	0.061	0.18	20.22	8.6	0.8253	0.90	1
026_U		217333	1.4	0.49	0.14	4.348	7.4	0.8290	0.47	1
027_U		45280	4.3	0.12	0.36	54.80	4.0	0.8014	0.75	1
028_U		106376	4.2	0.26	0.36	25.85	6.8	0.8208	0.63	1
029_U		46138	1.1	0.11	0.52	15.40	9.0	0.8247	0.85	1
030_U		143271	1.3	0.31	0.098	6.515	12	0.8286	0.50	1
031_U		104559	1.0	0.26	0.14	6.336	3.5	0.8281	0.56	1
032_U		66441	0.94	0.15	0.33	9.637	5.2	0.8307	0.78	1
033_U		40961	1.8	0.099	0.12	28.05	4.8	0.8213	0.76	1
034_U		14702	1.1	0.035	0.12	47.15	5.1	0.7992	1.6	1
035_U		28122	1.1	0.067	0.066	24.78	10	0.8136	0.87	1
036_U		42203	0.59	0.10	0.081	9.232	9.2	0.8277	0.71	1
037_U		164255	1.1	0.37	0.14	4.766	15	0.8291	0.53	1
038_U		260017	1.8	0.49	0.098	5.783	11	0.8302	0.47	1
039_U		27954	1.1	0.054	0.24	30.81	5.5	0.8191	0.83	1
040_U		59629	0.96	0.13	0.69	11.90	3.6	0.8280	0.65	1
041_U		20142	1.2	0.047	0.064	39.23	11	0.8030	1.1	1
042_U		172098	0.87	0.46	0.33	2.984	12	0.8315	0.51	1
043_U		26953	0.61	0.040	0.040	24.13	8.6	0.8164	0.98	1
044_U		25995	1.1	0.063	0.15	27.36	5.9	0.8133	1.1	1
045_U		30038	0.94	0.071	0.15	20.81	12	0.8210	1.0	1
046_U		416821	0.98	0.73	0.071	2.138	27	0.8309	0.46	1
047_U		27537	1.6	0.050	0.34	49.55	9.3	0.7956	1.1	1
048_U		34116	1.5	0.083	0.23	28.89	3.3	0.8144	0.76	1
049_U		9837	1.2	0.023	0.10	80.08	3.2	0.7825	1.2	1
050_U		17639	5.7	0.054	0.031	158.0	6.9	0.7188	1.3	1
059_U		60318	1.9	0.15	0.20	20.29	5.9	0.8131	0.82	1
060_U		14510	1.1	0.030	0.10	57.79	5.7	0.7979	1.1	1
061_U		99693	0.90	0.23	0.098	6.175	11	0.8280	0.64	1
062_U		106403	1.4	0.23	0.078	9.364	6.6	0.8275	0.54	1
063_U		33943	1.4	0.049	0.19	43.08	8.4	0.7970	1.1	1
067_U		9178	0.25	0.019	0.19	20.53	4.6	0.8202	1.4	1
068_U		60040	3.4	0.14	0.063	37.77	7.1	0.8103	0.71	1
069_U		42920	3.3	0.11	0.060	47.99	6.5	0.8031	0.78	1
070_U		71312	2.1	0.18	0.069	18.77	8.0	0.8194	0.73	1
071_U		16427	1.6	0.040	0.036	60.56	6.5	0.7900	1.4	1
009_U	BCR 9644	1031	0.061	0.001	0.012	74.49	7.0	0.8324	3.9	2
010_U		87	0.006	0.000	0.0056	68.34	11	0.8105	13	2
011_U		87	0.014	0.000	-0.00112	156.2	10	0.7736	14	2
014_U		110	0.020	0.000	0.0083	243.5	9.5	0.7783	13	2
015_U		343	0.016	0.000	0.0030	108.7	9.3	0.8263	8.4	2
017_U		337	0.036	0.000	-0.00574	130.1	9.7	0.8259	7.1	2
018_U		125	0.025	0.000	-0.00418	220.6	9.0	0.7825	11	2
019_U		275	0.019	0.000	-0.02679	201.2	9.5	0.7862	10	2
021_U		109	0.025	0.000	0.0081	217.8	8.9	0.7236	11	2
022_U		470	0.029	0.000	0.0089	240.5	9.8	0.7104	8.7	2
023_U		108	0.019	0.000	0.0084	206.7	9.9	0.7573	12	2
024_U		141	0.030	0.000	0.0024	246.3	8.1	0.8004	11	2
025_U		720	0.045	0.001	-0.00528	119.5	6.9	0.8306	5.4	2
026_U		347	0.038	0.001	0.046	117.3	8.2	0.7971	6.9	2



300 Table 5: continue...

027_U	1796	0.57	0.002	0.0067	488.8	19	0.6571	4.2	2	
028_U	2103	0.020	0.003	0.032	9.585	9.5	0.8217	2.9	2	
029_U	2505	0.62	0.002	0.0018	577.5	21	0.6308	5.7	2	
031_U	285	0.030	0.000	0.010	109.3	6.5	0.7944	7.0	2	
032_U	1114	0.19	0.001	0.0056	247.8	6.6	0.7212	4.3	2	
033_U	148	0.059	0.000	0.0095	360.8	8.7	0.6898	11	2	
034_U	180	0.017	0.000	0.014	106.2	9.4	0.7711	9.8	2	
035_U	73633	0.30	0.025	0.0011	19.18	36	0.8220	0.93	2	
036_U	200	0.006	0.000	0.043	30.98	11	0.8088	8.4	2	
037_U	925	0.10	0.002	0.00099	73.86	21	0.8161	5.5	2	
039_U	406	0.068	0.001	0.0050	164.1	8.8	0.7734	6.3	2	
350_U	9048	0.48	0.016	0.019	46.44	7.7	0.8196	1.5	2	
359_U	50690	0.64	0.079	0.057	12.70	11	0.8247	0.66	2	
360_U	5648	0.62	0.009	0.0088	109.5	5.9	0.7752	1.9	2	
361_U	1218	0.11	0.002	0.0097	82.26	8.4	0.7972	4.1	2	
365_U	49349	0.54	0.061	0.039	14.14	9.0	0.8213	0.72	2	
366_U	4943	0.040	0.007	0.018	8.691	21	0.8239	2.5	2	
368_U	1226	0.021	0.002	0.058	17.45	8.1	0.8227	3.5	2	
369_U	65958	0.25	0.12	0.11	3.320	13	0.8291	0.62	2	
374_U	305	0.032	0.001	-0.00810	92.10	7.1	0.7948	7.8	2	
375_U	2308	0.087	0.003	0.014	52.37	12	0.8094	4.9	2	
376_U	27934	0.78	0.032	0.020	38.35	11	0.8195	0.89	2	
377_U	17604	1.0	0.035	0.0051	44.70	10	0.8127	1.0	2	
378_U	58189	0.63	0.082	0.012	12.09	15	0.8195	0.62	2	
382_U	9122	0.93	0.015	0.0072	96.07	5.6	0.7875	1.5	2	
384_U	882	0.019	0.001	0.099	21.28	18	0.8240	4.5	2	
387_U	6049	0.32	0.008	0.010	61.42	13	0.8097	1.8	2	
388_U	6781	0.52	0.010	0.0076	79.65	11	0.8000	1.6	2	
389_U	6780	1.2	0.010	0.0023	182.9	11	0.7553	2.3	2	
390_U	17237	0.90	0.028	0.015	50.27	6.2	0.8145	1.1	2	
391_U	1518	0.11	0.002	0.0077	74.06	10	0.8176	3.3	2	
392_U	6719	0.40	0.008	0.0075	82.20	4.7	0.7937	1.7	2	
160_U	MTO 4-4	42459	0.071	0.033	0.12	3.455	16	0.8322	0.76	2
161_U		36404	0.100	0.024	0.086	6.599	10	0.8274	0.80	2
162_U		29300	0.31	0.025	0.12	19.64	15	0.8157	0.81	2
164_U		107586	0.65	0.064	0.11	16.10	12	0.8229	0.62	2
166_U		62776	1.1	0.055	0.13	32.05	4.3	0.8194	1.1	2
167_U		111666	0.47	0.12	0.16	6.312	15	0.8264	0.55	2
168_U		86330	0.82	0.076	0.12	17.08	7.0	0.8159	0.59	2
169_U		361703	0.88	0.24	0.10	5.739	15	0.8268	0.43	2
170_U		635386	0.50	0.56	0.14	1.426	11	0.8318	0.49	2
171_U		124867	0.27	0.083	0.11	5.252	16	0.8296	0.55	2
174_U		39215	0.67	0.032	0.075	33.18	9.4	0.8066	0.78	2
177_U		51601	0.29	0.049	0.11	9.368	8.3	0.8236	0.72	2
178_U		109476	1.3	0.079	0.093	26.16	11	0.8123	0.60	2
179_U		239957	0.80	0.19	0.12	6.474	9.5	0.8249	0.47	2
180_U		296212	0.93	0.23	0.13	6.498	15	0.8244	0.45	2
181_U		361123	0.98	0.35	0.082	4.497	13	0.8251	0.43	2
182_U		178465	0.91	0.12	0.14	12.41	5.1	0.8252	0.51	2
183_U		39048	0.49	0.037	0.067	21.37	8.1	0.8182	0.96	2
184_U		1048150	0.65	0.94	0.046	1.089	3.9	0.8279	0.39	2
185_U		102247	0.84	0.090	0.10	14.76	8.1	0.8206	0.61	2
186_U		121692	1.0	0.11	0.10	14.40	5.0	0.8202	0.50	2
187_U		198711	0.62	0.14	2.61	6.826	7.4	0.8273	0.47	2
188_U		291589	1.2	0.27	0.11	6.743	6.3	0.8238	0.43	2
189_U		231299	1.1	0.18	0.14	9.687	8.5	0.8269	0.45	2
190_U		413220	0.81	0.35	0.12	3.665	5.6	0.8296	0.42	2
191_U		11917	0.074	0.008	0.14	13.84	9.4	0.8215	1.4	2
192_U		126152	0.96	0.12	0.092	12.84	11	0.8217	0.62	2
193_U		73154	0.75	0.062	0.29	19.21	10	0.8187	0.86	2
194_U		549529	0.61	0.49	0.13	1.982	12	0.8351	0.45	2
197_U		51681	0.30	0.046	0.32	10.41	9.6	0.8230	0.72	2
198_U		273244	0.68	0.23	0.20	4.658	9.0	0.8330	0.45	2
209_U		477618	0.84	0.36	0.12	3.646	17	0.8277	0.41	2
210_U		412526	1.0	0.30	0.10	5.471	9.2	0.8287	0.43	2



Table 5: continue...

211_U	293172	1.0	0.18	0.13	8.843	11	0.8263	0.45	2
212_U	555903	1.1	0.38	0.088	4.670	16	0.8287	0.41	2
213_U	76097	0.92	0.047	0.084	31.17	8.0	0.8095	0.68	2
214_U	346163	1.1	0.31	0.23	5.896	6.1	0.8265	0.43	2
215_U	120901	0.90	0.10	0.11	14.03	14	0.8228	0.53	2
217_U	262806	1.3	0.35	0.13	5.921	8.3	0.8314	0.44	2
219_U	127957	1.0	0.10	0.13	16.17	13	0.8172	0.58	2
220_U	7919	0.11	0.004	0.16	42.58	11	0.8090	1.8	2
221_U	148260	1.6	0.13	0.24	19.25	5.8	0.8175	0.48	2
222_U	128181	1.3	0.094	0.089	20.96	13	0.8179	0.55	2
223_U	307635	1.5	0.26	0.14	9.247	4.3	0.8249	0.44	2
225_U	254729	1.6	0.23	0.11	11.19	8.6	0.8251	0.48	2
226_U	355548	1.3	0.24	0.11	8.578	9.1	0.8241	0.43	2
227_U	156455	1.1	0.14	0.098	12.89	7.5	0.8222	0.50	2
228_U	681461	0.67	0.64	0.095	1.651	10	0.8295	0.45	2
229_U	95834	1.0	0.084	0.10	19.44	7.7	0.8180	0.57	2
231_U	157487	1.3	0.14	0.081	13.86	12	0.8220	0.50	2
232_U	3039	0.066	0.003	0.16	33.96	7.1	0.8091	3.0	2
233_U	118467	2.0	0.10	0.060	30.51	7.1	0.8138	0.51	2
234_U	133809	1.6	0.11	0.12	23.19	8.0	0.8166	0.52	2
235_U	168534	1.8	0.15	0.10	19.46	6.0	0.8155	0.52	2
236_U	220800	1.8	0.19	0.18	14.73	11	0.8218	0.47	2
237_U	246643	1.3	0.21	0.084	9.590	7.9	0.8252	0.46	2
238_U	379877	0.62	0.29	0.089	3.429	32	0.8280	0.44	2
239_U	217983	0.78	0.19	0.11	6.434	14	0.8287	0.49	2
240_U	412692	0.73	0.38	0.066	3.048	12	0.8311	0.45	2
241_U	48316	0.51	0.040	0.15	20.14	7.7	0.8204	0.64	2
244_U	MTO 11-3 31010	0.020	0.020	2.18	1.605	14	0.8367	1.0	2
245_U	24767	0.047	0.030	0.53	2.522	22	0.8298	0.98	2
247_U	63055	0.28	0.079	0.38	5.659	7.2	0.8300	0.68	2
248_U	99922	0.26	0.13	0.53	3.038	5.8	0.8329	0.55	2
249_U	16054	0.064	0.024	0.59	4.306	7.1	0.8338	1.1	2
250_U	95971	0.20	0.094	0.47	3.360	5.4	0.8268	0.57	2
259_U	20407	0.83	0.026	0.11	50.50	12	0.7972	1.1	2
260_U	1786	0.011	0.003	0.74	6.092	8.0	0.8376	3.1	2
265_U	124037	0.14	0.10	0.95	2.202	8.5	0.8317	0.55	2
266_U	19405	0.088	0.021	0.47	6.703	14	0.8330	1.0	2
268_U	145975	1.7	0.21	0.21	12.39	7.1	0.8255	0.58	2
269_U	136367	0.12	0.19	1.64	1.023	5.3	0.8312	0.51	2
271_U	12070	0.034	0.018	1.15	2.977	14	0.8323	1.2	2
272_U	55571	0.22	0.075	0.45	4.556	5.9	0.8267	0.65	2
274_U	9126	0.059	0.012	0.55	7.695	11	0.8312	2.2	2
275_U	11007	0.054	0.017	1.23	5.116	6.3	0.8262	1.2	2
276_U	58251	0.092	0.080	0.54	1.841	16	0.8373	0.67	2
277_U	112321	0.29	0.13	1.17	3.413	8.0	0.8274	0.55	2
278_U	18070	0.048	0.028	0.75	2.698	7.3	0.8292	0.93	2
279_U	105781	0.37	0.15	0.69	3.774	6.9	0.8304	0.54	2
281_U	153346	4.0	0.22	0.081	28.52	7.9	0.8107	0.51	2
282_U	141144	3.6	0.20	0.069	27.90	8.6	0.8121	0.52	2
283_U	70729	0.71	0.11	0.15	9.890	4.2	0.8229	0.59	2
284_U	57878	0.28	0.065	0.32	6.812	14	0.8344	0.67	2
285_U	179536	0.73	0.19	0.34	6.075	4.7	0.8349	0.48	2
286_U	201969	1.3	0.32	0.31	6.386	4.9	0.8261	0.44	2
287_U	374142	2.5	0.56	0.055	7.103	7.0	0.8247	0.42	2
288_U	128171	3.2	0.18	0.087	28.71	5.0	0.8112	0.58	2
289_U	136966	4.1	0.18	0.082	35.20	5.3	0.8090	0.53	2
290_U	107867	4.9	0.16	0.060	48.17	7.7	0.8005	0.57	2
291_U	106011	1.9	0.17	0.43	17.90	18	0.8193	0.65	2
292_U	61587	4.5	0.11	0.075	63.75	15	0.7965	1.1	2
293_U	91650	3.8	0.14	0.043	42.71	5.7	0.8084	0.58	2
294_U	80760	3.8	0.12	0.075	47.86	5.8	0.8000	0.66	2
295_U	67617	4.3	0.11	0.043	62.75	5.6	0.7921	0.67	2
436_U	Pu 05 1336	0.008	0.001	0.018	17.15	12	0.7968	3.4	2
440_U	3541	0.013	0.002	0.047	9.396	12	0.7993	3.3	2
441_U	5779	0.013	0.001	0.089	18.43	9.4	0.7958	2.4	2



Table 5: continue...

442_U	819	0.010	0.000	0.0016	36.21	12	0.7929	4.3	2	
444_U	3503	0.002	0.001	0.058	5.613	15	0.7931	2.7	2	
445_U	1398	0.006	0.001	0.043	12.30	8.4	0.7884	3.4	2	
463_U	2058	0.019	0.001	0.043	19.92	10	0.7828	3.4	2	
464_U	2093	0.019	0.001	0.059	23.30	7.5	0.7863	2.9	2	
465_U	1188	0.007	0.001	0.12	16.62	13	0.7885	4.6	2	
466_U	7720	0.049	0.005	0.043	14.59	4.8	0.7909	1.6	2	
467_U	2652	0.032	0.002	0.032	26.36	15	0.7822	3.6	2	
468_U	51097	0.31	0.030	0.045	15.94	4.4	0.7918	0.65	2	
469_U	39483	0.30	0.024	0.13	19.22	4.7	0.7889	0.77	2	
470_U	18990	0.23	0.011	0.031	33.65	6.1	0.7832	0.96	2	
472_U	77384	0.56	0.046	0.022	18.78	5.0	0.7925	0.58	2	
473_U	42753	1.2	0.029	0.014	62.46	7.5	0.7622	0.78	2	
474_U	38267	0.51	0.026	0.017	29.85	12	0.7871	0.98	2	
475_U	6462	0.25	0.004	0.0099	92.20	9.6	0.7538	2.3	2	
476_U	55482	0.93	0.039	0.092	36.70	9.8	0.7884	0.89	2	
477_U	24674	0.11	0.016	0.047	11.19	4.7	0.7968	1.0	2	
478_U	2847	0.075	0.002	0.0068	74.37	12	0.7544	2.4	2	
479_U	70165	0.52	0.045	0.079	17.80	6.7	0.7906	0.60	2	
480_U	184870	0.88	0.12	0.069	11.87	3.8	0.7968	0.48	2	
481_U	11662	0.62	0.008	0.0093	115.9	7.6	0.7352	1.2	2	
483_U	1829	0.014	0.001	0.030	15.84	11	0.7971	3.2	2	
486_U	652	0.003	0.001	0.032	8.749	22	0.7941	5.5	2	
487_U	97239	1.4	0.060	0.019	36.73	4.6	0.7742	0.57	2	
488_U	12860	0.70	0.009	0.0061	122.2	8.9	0.7343	1.4	2	
489_U	22723	0.84	0.014	0.011	89.94	4.9	0.7468	0.93	2	
490_U	39877	0.51	0.026	0.013	30.42	6.1	0.7844	0.81	2	
491_U	30830	1.0	0.014	0.016	114.4	16	0.7368	0.91	2	
492_U	19082	1.0	0.014	0.013	106.9	10	0.7335	1.1	2	
009_U	MTO 11-3	90036	2.9	0.29	0.14	31.54	10	0.8054	0.65	3
010_U	60711	4.8	0.19	0.058	80.09	4.6	0.7784	0.73	3	
011_U	321269	3.1	0.97	0.36	10.25	6.6	0.8207	0.40	3	
012_U	18890	1.8	0.061	0.081	92.39	6.5	0.7715	1.1	3	
013_U	104308	2.0	0.32	0.12	20.01	8.7	0.8134	0.49	3	
014_U	49427	2.4	0.13	0.076	72.22	11	0.7788	0.99	3	
015_U	140824	4.3	0.43	0.14	32.07	4.3	0.8054	0.50	3	
017_U	107005	3.6	0.34	0.083	34.10	5.5	0.8103	0.54	3	
018_U	63650	0.60	0.19	0.30	10.74	7.3	0.8207	0.60	3	
024_U	112992	0.55	0.35	0.92	5.077	9.5	0.8279	0.48	3	
025_U	148314	0.57	0.45	0.77	4.294	9.0	0.8277	0.44	3	
028_U	148368	3.1	0.40	0.11	29.45	11	0.8088	0.60	3	
031_U	54347	2.1	0.17	0.075	42.55	8.5	0.7968	0.76	3	
033_U	158602	3.3	0.50	0.23	21.72	4.9	0.8142	0.45	3	
034_U	47147	0.31	0.14	0.38	7.791	5.9	0.8239	0.66	3	
035_U	161917	3.2	0.50	0.34	20.44	5.5	0.8167	0.42	3	
037_U	245790	3.2	0.68	0.23	17.08	6.7	0.8149	0.47	3	
038_U	152560	4.6	0.48	0.14	30.05	6.2	0.8048	0.54	3	
040_U	45567	2.2	0.14	0.11	50.70	5.5	0.7961	0.68	3	
041_U	43416	0.35	0.14	0.43	8.464	8.0	0.8208	0.94	3	
042_U	41614	0.27	0.13	0.39	7.039	7.3	0.8276	0.77	3	
043_U	51784	0.32	0.16	0.43	6.705	5.5	0.8184	0.67	3	
044_U	185745	4.0	0.53	0.19	26.15	8.7	0.8085	0.46	3	
045_U	197622	1.6	0.58	0.12	9.503	18	0.8224	0.45	3	
046_U	163159	3.2	0.52	0.15	19.59	7.1	0.8129	0.52	3	
047_U	137303	3.2	0.45	0.17	21.78	6.0	0.8140	0.54	3	
048_U	74586	3.5	0.24	0.098	47.14	5.7	0.7992	0.63	3	
049_U	142496	4.4	0.45	0.14	31.29	4.5	0.8067	0.43	3	
050_U	148349	4.8	0.45	0.14	36.35	6.6	0.8066	0.51	3	
059_U	102822	3.0	0.32	0.18	30.04	6.2	0.8036	0.51	3	
061_U	125428	3.2	0.40	0.16	25.59	6.9	0.8108	0.47	3	
062_U	37071	1.1	0.13	0.13	23.38	9.8	0.8098	0.76	3	
063_U	48032	0.78	0.16	0.12	15.90	6.3	0.8180	0.71	3	
064_U	69242	0.51	0.21	0.58	8.442	13	0.8203	0.63	3	
065_U	165434	4.1	0.51	0.060	26.34	9.2	0.8096	0.53	3	
066_U	134214	5.5	0.42	0.085	41.66	9.2	0.7982	0.55	3	



Table 5: continue...

067_U		35032	3.5	0.12	0.051	91.67	4.7	0.7642	0.82	3
068_U		197102	2.8	0.65	0.17	13.21	5.2	0.8204	0.40	3
069_U		152700	2.9	0.46	0.12	21.30	17	0.8147	0.57	3
071_U		108748	0.34	0.35	1.35	3.081	9.5	0.8266	0.52	3
072_U		170691	0.85	0.55	0.59	4.946	11	0.8292	0.52	3
073_U		9935	1.7	0.032	0.068	155.2	7.0	0.7228	1.5	3
074_U		92588	5.5	0.30	0.059	58.10	9.9	0.7929	0.77	3
009_U	Pu 05	2167	0.030	0.002	0.0045	64.40	17	0.7620	3.1	4
011_U		642	0.003	0.001	0.018	12.15	16	0.8304	6.2	4
013_U		2053	0.002	0.002	0.062	4.612	6.6	0.8177	2.8	4
014_U		550	0.011	0.000	0.0052	75.72	18	0.7705	7.0	4
015_U		1351	0.027	0.001	0.00067	67.07	8.5	0.7705	3.5	4
016_U		7081	0.10	0.006	0.015	56.46	7.6	0.7632	1.6	4
017_U		2027	0.064	0.002	0.0088	132.8	9.8	0.7411	2.8	4
018_U		1355	0.051	0.001	0.0042	127.1	15	0.7475	3.5	4
019_U		9372	0.10	0.007	0.018	63.09	8.6	0.7824	2.2	4
020_U		2028	0.015	0.002	0.013	27.00	6.9	0.7825	3.0	4
021_U		3008	0.011	0.002	0.0037	18.46	5.1	0.8120	2.8	4
022_U		1140	0.005	0.001	0.0098	13.19	19	0.7949	4.4	4
023_U		1051	0.033	0.001	0.0029	94.71	16	0.7526	4.8	4
025_U		4316	0.059	0.004	0.0071	51.96	14	0.7794	1.9	4
026_U		7481	0.050	0.007	0.022	23.39	9.4	0.7891	1.6	4
027_U		6387	0.028	0.006	0.010	12.93	18	0.7951	1.7	4
028_U		12431	0.023	0.011	0.0018	6.389	14	0.8304	1.3	4
029_U		1118	0.023	0.001	0.0070	73.49	9.6	0.7553	4.8	4
030_U		1099	0.004	0.001	0.00034	6.039	35	0.8159	3.8	4
031_U		2456	0.003	0.002	0.029	4.920	11	0.8120	2.5	4
032_U		8610	0.057	0.007	0.042	29.39	9.7	0.7989	1.8	4
033_U		2450	0.006	0.002	0.086	8.355	7.5	0.8029	3.9	4
034_U		1943	0.010	0.001	0.029	22.89	6.7	0.8047	3.3	4
037_U		1471	0.010	0.001	0.014	23.40	12	0.8005	4.0	4
038_U		4241	0.057	0.003	0.0077	79.29	9.5	0.7796	2.4	4
040_U		5569	0.039	0.005	0.049	25.95	6.2	0.8039	1.8	4
041_U		2789	0.008	0.002	0.015	10.48	20	0.8099	2.3	4
042_U		2272	0.022	0.002	0.0071	35.64	20	0.8083	2.9	4
043_U		845	0.006	0.001	0.017	16.92	20	0.8020	4.5	4
044_U		1053	0.002	0.001	0.046	8.587	15	0.8135	3.7	4
045_U		2058	0.004	0.002	0.023	6.070	8.1	0.8143	2.8	4
046_U		1004	0.003	0.001	0.018	14.56	9.9	0.7973	3.8	4
047_U		1329	0.016	0.001	0.00077	33.81	31	0.8012	3.7	4
048_U		1422	0.021	0.001	0.0060	45.24	15	0.7810	3.1	4
049_U		276573	1.2	0.16	0.049	37.36	12	0.7884	0.56	4
060_U		1411	0.006	0.001	0.0053	15.00	12	0.8117	3.0	4
061_U		7356	0.090	0.005	0.084	81.01	27	0.7538	2.1	4
062_U		1435	0.043	0.001	0.0064	117.0	14	0.7277	3.2	4
064_U		633	0.056	0.001	0.0010	219.2	23	0.6783	5.8	4
067_U		108576	0.66	0.094	0.019	21.24	4.2	0.8007	0.55	4
068_U		22860	0.23	0.019	0.017	37.25	4.5	0.7906	0.91	4
073_U		2091	0.14	0.002	0.0021	199.1	9.7	0.6805	3.3	4
075_U		748	0.007	0.001	0.0033	29.09	18	0.8043	4.8	4
078_U		1316	0.061	0.001	0.0023	150.7	9.0	0.7338	3.7	4
079_U		2405	0.044	0.002	0.0056	60.40	15	0.7854	2.5	4
080_U		2285	0.032	0.002	0.0047	46.32	13	0.7933	2.8	4
081_U		2198	0.040	0.002	0.011	78.19	6.2	0.7541	2.5	4
088_U	MTO 4-4	154270	1.5	0.23	0.24	22.94	8.6	0.8128	0.51	4
089_U		66593	1.0	0.11	0.075	31.35	8.3	0.8050	0.64	4
092_U		25818	0.94	0.043	0.14	72.14	9.5	0.7867	1.3	4
093_U		188855	1.5	0.29	0.15	18.28	12	0.8136	0.45	4
094_U		70717	1.5	0.12	0.099	42.66	3.3	0.7971	0.68	4
095_U		392652	1.3	0.68	0.14	5.799	17	0.8244	0.40	4
096_U		39333	0.54	0.065	0.14	27.02	9.7	0.8107	0.72	4
098_U		343014	0.64	0.58	0.33	3.486	9.0	0.8302	0.43	4
099_U		15397	0.083	0.027	0.36	9.619	12	0.8195	1.2	4
100_U		35522	0.27	0.060	0.24	14.65	4.5	0.8160	0.78	4
109_U		202639	1.6	0.34	0.081	14.63	19	0.8141	0.57	4



Table 5: continue...

110_U		42283	0.70	0.069	0.083	33.87	5.6	0.8050	0.75	4
111_U		112583	1.5	0.19	0.099	25.52	9.2	0.8088	0.50	4
112_U		120520	0.70	0.21	0.043	10.44	16	0.8226	0.54	4
113_U		4129	0.17	0.007	0.067	75.44	9.7	0.7836	2.3	4
114_U		64831	0.23	0.12	0.051	6.233	6.3	0.8270	0.63	4
115_U		386587	2.3	0.63	0.061	11.80	8.6	0.8204	0.36	4
116_U		101833	0.059	0.18	0.59	1.008	20	0.8328	0.51	4
117_U		36664	0.023	0.066	0.93	1.063	21	0.8262	0.80	4
118_U		263914	1.5	0.45	0.11	10.72	10	0.8204	0.42	4
119_U		198490	1.0	0.33	0.16	10.32	10	0.8199	0.46	4
120_U		321214	1.3	0.54	0.099	7.662	5.1	0.8241	0.38	4
121_U		77903	0.53	0.13	0.046	12.56	6.3	0.8208	0.64	4
122_U		477392	1.1	0.81	0.13	4.040	11	0.8258	0.43	4
123_U		62459	0.84	0.11	0.089	25.60	12	0.8143	0.66	4
124_U		83446	0.45	0.14	0.13	9.875	14	0.8151	0.56	4
125_U		328913	0.86	0.53	0.11	5.216	11	0.8267	0.38	4
126_U		51257	1.2	0.080	0.082	53.19	6.5	0.7948	0.88	4
127_U		165366	1.2	0.28	0.094	13.05	6.3	0.8199	0.44	4
128_U		128085	0.78	0.24	0.14	9.825	15	0.8209	0.48	4
129_U		40122	0.48	0.068	0.076	22.54	8.6	0.8123	0.72	4
130_U		243432	1.6	0.40	0.11	12.91	8.9	0.8182	0.41	4
131_U		410018	1.0	0.63	0.098	5.566	9.6	0.8252	0.38	4
132_U		453513	1.3	0.75	0.11	5.295	13	0.8225	0.39	4
133_U		140762	1.0	0.23	0.10	14.54	10	0.8205	0.45	4
134_U		171451	1.8	0.25	0.11	27.07	5.9	0.8110	0.49	4
135_U		299485	1.3	0.50	0.088	8.646	7.3	0.8253	0.40	4
136_U		273271	0.95	0.46	0.13	6.742	7.5	0.8255	0.38	4
137_U		261422	1.00	0.44	0.17	7.251	8.8	0.8219	0.40	4
139_U		336303	1.2	0.56	0.20	6.730	14	0.8277	0.38	4
140_U		91664	0.34	0.15	0.11	7.230	15	0.8242	0.51	4
141_U		2833	0.13	0.005	0.16	98.39	7.1	0.7727	3.4	4
143_U		178759	0.87	0.30	0.089	9.142	10	0.8233	0.44	4
144_U		175078	1.1	0.30	0.10	11.67	18	0.8186	0.50	4
145_U		190119	1.2	0.30	0.11	13.46	8.7	0.8178	0.46	4
146_U		85820	1.4	0.15	0.22	30.20	3.5	0.8081	0.62	4
147_U		329223	0.75	0.55	0.14	4.281	9.5	0.8254	0.40	4
148_U		114269	1.1	0.20	0.094	18.16	8.5	0.8142	0.53	4
149_U		248241	1.1	0.42	0.10	8.312	8.3	0.8215	0.41	4
150_U		181792	0.92	0.28	0.100	11.66	10.0	0.8192	0.47	4
159_U		122725	0.83	0.21	0.17	12.59	5.4	0.8211	0.48	4
160_U		126548	0.90	0.22	0.10	12.68	8.3	0.8214	0.50	4
161_U		110684	1.9	0.17	0.086	39.06	4.6	0.8017	0.58	4
162_U		78280	1.2	0.13	0.092	30.26	7.1	0.8049	0.71	4
165_U		195480	1.0	0.34	0.092	9.686	9.0	0.8209	0.44	4
166_U		303135	1.3	0.49	0.11	8.744	7.7	0.8241	0.40	4
169_U		62163	0.87	0.11	0.079	22.90	9.7	0.8160	0.62	4
170_U		124538	1.1	0.21	0.093	17.94	7.9	0.8174	0.45	4
171_U		156199	1.3	0.27	0.089	15.78	13	0.8168	0.46	4
172_U		58090	0.92	0.094	0.090	33.53	7.6	0.8049	0.63	4
173_U		88433	1.5	0.14	0.10	40.49	7.9	0.7982	0.53	4
175_U		70717	1.1	0.11	0.100	34.96	6.1	0.8048	0.71	4
176_U		115260	1.2	0.15	0.099	39.42	5.0	0.8018	0.75	4
177_U		35514	0.82	0.058	0.079	47.42	5.3	0.7983	0.80	4
178_U		60006	1.5	0.090	0.095	59.06	8.5	0.7877	0.77	4
179_U		263568	1.7	0.45	0.091	11.81	9.8	0.8172	0.51	4
180_U		237512	1.2	0.38	0.089	10.36	26	0.8202	0.53	4
181_U		79587	1.0	0.14	0.12	24.39	5.7	0.8099	0.56	4
182_U		181676	1.5	0.31	0.16	15.23	8.6	0.8179	0.49	4
183_U		148496	0.62	0.39	0.15	3.828	6.4	0.8256	0.42	4
184_U		338583	1.7	0.59	0.067	9.117	8.8	0.8256	0.39	4
185_U		79508	1.1	0.13	0.065	26.54	4.1	0.8143	0.56	4
186_U		85236	0.73	0.15	0.089	15.83	9.9	0.8170	0.54	4
187_U		307851	1.0	0.53	0.26	5.904	13	0.8191	0.43	4
188_U		116771	1.1	0.21	0.087	16.25	11	0.8141	0.53	4
280_U	BOX 108	3723	0.027	0.015	0.018	4.210	34	0.8405	2.5	4



310 Table 5: continue...

283_U	215245	2.5	0.52	0.12	19.76	7.4	0.8240	0.47	4
284_U	95417	1.1	0.28	0.14	13.04	4.9	0.8259	0.51	4
287_U	9849	1.3	0.030	0.033	133.6	4.0	0.7471	1.5	4
288_U	11288	1.5	0.035	0.042	124.2	4.9	0.7493	1.6	4
289_U	34194	0.096	0.099	0.22	3.185	13	0.8344	0.81	4
290_U	242588	2.0	0.72	0.18	8.867	7.6	0.8307	0.42	4
291_U	142226	1.3	0.40	0.11	10.56	12	0.8321	0.45	4
292_U	205563	1.8	0.52	0.11	13.32	8.8	0.8231	0.44	4
293_U	174825	1.0	0.41	0.054	11.00	18	0.8305	0.45	4
294_U	155002	1.8	0.44	0.15	14.07	3.5	0.8248	0.46	4
296_U	135623	1.4	0.34	0.25	16.69	9.9	0.8252	0.47	4
297_U	431598	1.3	1.1	0.34	4.623	9.7	0.8293	0.37	4
298_U	73380	1.8	0.22	0.027	26.06	9.7	0.8186	0.58	4
299_U	285598	2.7	0.76	0.012	12.45	7.6	0.8291	0.43	4
300_U	177111	1.4	0.51	0.14	8.972	13	0.8245	0.46	4
309_U	20078	0.082	0.061	0.23	4.368	34	0.8415	1.4	4
311_U	162504	1.2	0.49	0.14	7.592	13	0.8274	0.50	4
312_U	300617	2.1	0.89	0.22	7.673	8.5	0.8305	0.42	4
313_U	4524	0.035	0.013	0.061	8.581	14	0.8286	2.2	4
314_U	149794	0.98	0.42	0.16	8.132	5.8	0.8278	0.46	4
315_U	151082	2.8	0.45	0.15	20.25	3.9	0.8208	0.45	4
316_U	403090	5.0	1.2	0.066	13.02	7.7	0.8299	0.41	4
317_U	66022	1.6	0.20	0.15	25.40	4.4	0.8132	0.62	4
318_U	69901	1.3	0.21	0.10	21.32	15	0.8190	0.62	4
319_U	43921	2.7	0.13	0.062	68.54	9.7	0.7921	0.79	4
320_U	95589	0.99	0.30	0.26	10.46	3.5	0.8274	0.49	4
321_U	86168	0.84	0.26	0.21	10.38	11	0.8324	0.54	4
322_U	45837	0.39	0.13	0.079	11.04	8.6	0.8248	0.70	4
323_U	81816	1.1	0.25	0.14	14.89	3.8	0.8234	0.61	4
324_U	291563	2.1	0.88	0.11	7.571	16	0.8275	0.44	4
325_U	54488	2.5	0.17	0.066	46.74	9.2	0.8017	0.66	4
326_U	166955	1.6	0.51	0.035	10.17	5.0	0.8268	0.48	4
327_U	378811	0.73	1.1	0.18	2.132	9.8	0.8380	0.40	4
328_U	125856	2.6	0.40	0.035	19.49	20	0.8257	0.64	4
330_U	157915	2.0	0.45	0.074	15.73	9.3	0.8244	0.48	4
331_U	245854	1.8	0.66	0.29	9.850	7.9	0.8210	0.58	4
332_U	47905	0.41	0.12	0.15	12.59	9.9	0.8276	0.76	4
333_U	566996	4.6	1.7	0.12	8.640	9.0	0.8295	0.38	4
334_U	84562	1.2	0.25	0.096	16.17	3.2	0.8216	0.55	4
335_U	66581	1.8	0.19	0.12	31.10	8.8	0.8126	0.64	4
336_U	192058	3.3	0.54	0.056	21.03	5.8	0.8238	0.44	4
337_U	82708	1.7	0.25	0.14	21.94	5.4	0.8239	0.50	4
338_U	99827	2.1	0.30	0.19	22.02	6.9	0.8194	0.51	4
339_U	49540	1.6	0.15	0.091	33.08	11	0.8110	0.65	4
340_U	209779	1.5	0.61	0.14	8.328	28	0.8299	0.49	4
341_U	93794	0.90	0.26	0.086	11.96	6.9	0.8256	0.51	4
342_U	44297	1.6	0.12	0.051	50.34	5.0	0.7976	0.81	4
343_U	16242	0.025	0.049	0.36	1.664	30	0.8431	1.3	4
344_U	74235	0.35	0.21	0.30	5.544	4.8	0.8306	0.54	4
345_U	195664	1.3	0.54	0.11	8.889	6.4	0.8261	0.44	4
346_U	48143	0.61	0.12	0.15	22.81	3.8	0.8228	0.73	4
348_U	71996	0.59	0.20	0.094	10.79	4.2	0.8295	0.57	4
349_U	102507	1.1	0.30	0.26	12.24	15	0.8253	0.50	4
350_U	198463	2.5	0.51	0.035	18.76	9.3	0.8261	0.44	4
359_U	8939	0.043	0.024	0.45	6.144	27	0.8324	1.6	4
360_U	57033	0.98	0.17	0.24	18.08	9.6	0.8228	0.61	4
361_U	203520	4.3	0.62	0.069	22.01	12	0.8204	0.40	4
362_U	35763	2.9	0.11	0.038	80.60	6.4	0.7848	0.83	4
364_U	79345	1.4	0.25	0.083	17.82	4.7	0.8228	0.53	4
365_U	39697	2.2	0.12	0.096	59.48	4.7	0.7974	0.71	4
366_U	144201	0.82	0.43	0.12	6.093	16	0.8321	0.46	4
367_U	53472	0.69	0.16	0.088	13.48	8.2	0.8254	0.67	4
369_U	50693	2.5	0.16	0.10	49.25	7.4	0.7975	0.74	4
370_U	52833	2.4	0.17	0.076	44.69	6.3	0.8078	0.59	4
371_U	51179	0.82	0.16	0.11	16.64	14	0.8172	0.80	4



Table 5: continue...

372_U	14847	0.28	0.040	0.050	25.52	12	0.8150	1.3	4	
373_U	67995	0.55	0.20	0.083	8.701	13	0.8239	0.64	4	
374_U	169346	1.3	0.47	0.11	9.985	12	0.8279	0.45	4	
375_U	73258	1.4	0.23	0.11	19.10	10	0.8199	0.56	4	
376_U	30039	0.42	0.097	0.077	13.11	14	0.8220	0.77	4	
377_U	243980	1.9	0.75	0.15	8.114	4.6	0.8310	0.40	4	
378_U	28838	1.6	0.089	0.085	58.11	5.3	0.7966	0.95	4	
379_U	106946	2.6	0.33	0.039	24.87	5.1	0.8131	0.56	4	
380_U	64981	2.6	0.19	0.10	44.16	5.7	0.8001	0.62	4	
381_U	82318	2.1	0.21	0.091	39.33	13	0.8072	0.72	4	
382_U	78516	1.3	0.24	0.098	17.00	12	0.8192	0.59	4	
383_U	BCR 9644	22865	0.86	0.064	0.024	47.56	5.1	0.8056	0.97	4
384_U	6644	0.84	0.019	0.0040	146.9	11	0.7724	2.0	4	
386_U	77128	0.27	0.22	0.20	4.265	4.1	0.8256	0.55	4	
388_U	3416	0.41	0.011	0.016	114.6	4.8	0.7689	2.2	4	
390_U	18463	0.33	0.058	0.075	17.53	12	0.8061	1.0	4	
392_U	4305	0.14	0.008	0.0033	180.6	13	0.7574	3.8	4	
393_U	14388	1.3	0.044	0.016	91.44	5.8	0.7816	1.2	4	
394_U	18496	0.92	0.054	0.019	57.05	5.9	0.7943	1.1	4	
395_U	4428	0.20	0.012	0.041	58.79	5.9	0.8002	2.0	4	
396_U	12559	0.81	0.032	0.016	104.3	5.4	0.7788	1.5	4	
397_U	1342	0.59	0.004	0.0025	376.0	9.0	0.6875	4.7	4	
399_U	146754	0.20	0.32	0.11	3.469	6.1	0.8260	0.55	4	
409_U	11621	0.41	0.035	0.018	39.82	11	0.8117	1.5	4	
411_U	5627	0.48	0.018	0.021	84.35	7.9	0.7917	1.8	4	
412_U	23357	1.1	0.066	0.038	60.11	6.7	0.8029	0.97	4	
413_U	14314	0.22	0.041	0.061	19.04	15	0.8151	1.2	4	
415_U	6924	0.056	0.014	0.15	29.96	8.1	0.8014	4.3	4	
416_U	6828	0.17	0.020	0.026	28.80	8.2	0.8266	1.7	4	
423_U	4952	0.090	0.013	0.027	28.72	6.2	0.8009	2.2	4	
427_U	962	0.047	0.003	0.10	42.18	11	0.8056	4.0	4	
433_U	733	0.30	0.002	0.0013	444.8	12	0.6898	6.1	4	
435_U	3290	0.025	0.006	0.0021	35.94	17	0.8262	4.6	4	
438_U	1004	0.076	0.003	0.035	74.37	9.7	0.7965	4.1	4	
440_U	891	0.007	0.003	0.025	8.704	10	0.8189	4.4	4	
441_U	3306	0.47	0.010	0.0019	139.0	5.6	0.7832	2.1	4	
442_U	1782	0.18	0.005	0.0024	103.9	4.6	0.7908	3.0	4	
443_U	1876	0.10	0.005	0.0018	68.27	5.5	0.8084	2.9	4	
445_U	892	0.009	0.003	0.74	7.259	21	0.8357	4.3	4	
446_U	5383	0.20	0.017	0.0096	39.50	8.5	0.8110	1.6	4	
447_U	5316	0.36	0.016	0.0056	72.00	3.8	0.8105	1.7	4	
448_U	4019	0.44	0.013	0.0056	107.8	7.5	0.7851	3.3	4	
449_U	839	0.16	0.002	0.0045	235.9	9.6	0.7546	4.5	4	
450_U	27342	1.5	0.084	0.040	56.17	8.4	0.8088	1.0	4	
459_U	5280	0.17	0.017	0.016	31.91	19	0.8161	1.7	4	
462_U	37636	0.062	0.11	0.23	1.778	9.2	0.8254	0.80	4	
464_U	200339	2.3	0.61	0.050	11.77	6.9	0.8140	0.43	4	
467_U	676	0.005	0.002	0.74	9.950	9.0	0.8126	5.2	4	
468_U	1808	0.060	0.006	0.013	33.81	11	0.8128	3.0	4	
469_U	3923	0.13	0.013	0.17	29.07	15	0.8056	2.1	4	

^a Within run background-corrected mean ²⁰⁷Pb signal in cps (counts per second).

^b U and Pb concentrations and Th/U ratio were calculated relative to the primary reference material.

^c Corrected for background, within-run Pb/U fractionation (in case of ²⁰⁶Pb/²³⁸U) and subsequently normalised to the primary reference material (ID-TIMS value/measured value).

Author contributions

315 AB and AG were involved in the LA-ICPMS analysis and pit-depth measurements. IV accomplished the fieldwork and sample collection. All the authors collaborated in preparing the manuscript.



Competing interest

The authors declare that they have no conflict of interest.

Acknowledgements

- 320 FIERCE is financially supported by the Wilhelm and Else Heraeus Foundation and by the Deutsche Forschungsgemeinschaft (DFG, INST, 161/921-1 FUGG and INST 161/923-1 FUGG), which is gratefully acknowledged. Cores from Borehole EMS-4 (Cattolica Eraclea) in the Caltanissetta Basin (Sicily) are stored in the core repository of the University of Milano, Department of Earth Science “Ardito Desio” after core restoration performed within COST Action CA15103 MEDSALT.

References

- 325 Andreetto, F., Matsubara, K., Beets, C.J., Fortuin, A.R., Flecker, R., and Krijgsman, W.: High Mediterranean water-level during the Lago-Mare phase of the Messinian Salinity Crisis: insights from the Sr isotope records of Spanish marginal basins (SE Spain), *Paleogeogr. Paleoclimatol. Paleoecol.*, 562, 110139, <https://doi.org/10.1016/j.palaeo.2020.110139>, 2021.
- Astilleros, J.M., Godelitsas, A., Rodríguez-Blanco, J.D., Fernández-Díaz, L., Prieto, M., Lagoyannis, A., and Harissopulos, S.: Interaction of gypsum with Pb - bearing aqueous solutions, *Appl. Geochem.*, 25, 1008-1016.
- 330 <https://doi.org/10.1016/j.apgeochem.2010.04.007>, 2010.
- Babel, M., and Schreiber, B.C.: Geochemistry of evaporites and evolution of seawater, in: *Treatise on Geochemistry* (2nd edition), edited by: Turekian, K., and Holland, H., Elsevier, Oxford, UK, 483-560, <https://doi.org/10.1016/B978-0-08-095975-7.00718-X>, 2014.
- Brannon, J. C., Cole, S. C., Podosek, F. A., Ragan, V. M., Coveney, R. M., Wallace, M. W., and Bradley, A. J.: Th-Pb and U-
- 335 Pb dating of ore-stage calcite and Paleozoic fluid flow, *Science*, 271, 491-493, <https://doi.org/10.1126/science.271.5248.491>, 1996.
- Burisch, M., Walter, B. F. and Markl, G.: Silicification of Hydrothermal Gangue Minerals in Pb-Zn-Cu-Fluorite-Quartz-595 Baryte Veins, *The Canadian Mineralogist*, 55(3), 501-514, <https://doi.org/10.3749/canmin.1700005>, 2017.
- Burisch, M., Gerdes, A., Meinert, L., Albert, R., Seifert, T., and Gutzmer, J.: The essence of time - fertile skarn formation in
- 340 the Variscan Orogenic Belt, *Earth Planet. Sci. Lett.*, 519, 165-170, <https://doi.org/10.1016/j.epsl.2019.05.015>, 2019.
- CIESM: The Messinian salinity crisis from mega-deposits to microbiology, in: *A consensus report. 33ème CIESM Workshop Monographs 33*, edited by: Briand, F., CIESM Publisher, Monaco, 91-96, 2008.
- Clauer, N., Chaudhuri, S., Toulkeridis, T., and Blanc, G.: Fluctuations of Caspian Sea level: beyond climatic variations? *Geology*, 28, 1015–1018, [https://doi.org/10.1130/0091-7613\(2000\)28<1015:FOCSLB>2.0.CO;2](https://doi.org/10.1130/0091-7613(2000)28<1015:FOCSLB>2.0.CO;2), 2000.
- 345 Conley, R.F., and Bundy W.M.: Mechanism of gypsification, *Geochim. Cosmochim. Acta*, 15, 57-72, [https://doi.org/10.1016/0016-7037\(58\)90010-3](https://doi.org/10.1016/0016-7037(58)90010-3), 1958.



- Costanzo, A., Cipriani, M., Feely, M., Cianfione, G., and Dominici, R.: Messinian twinned selenite from the Catanzaro Trough, Calabria, Southern Italy: field, petrographic and fluid inclusion perspectives, *Carbonates and Evaporites*, 34, 743–756. <https://doi.org/10.1007/s13146-019-00516-0>, 2019.
- 350 Craig, G., Managh A.J., Stremtan, C., Lloyd, N.S., and Horstwood, M.S.A.: Doubling Sensitivity in Multicollector ICPMS Using High-Efficiency, Rapid Response Laser Ablation Technology, *Anal. Chem.*, 90, 11564–11571, <https://doi.org/10.1021/acs.analchem.8b02896>, 2018.
- Craig, G., Bracciali, L., and Lloyd, N.: LA-ICP-MS for U-(Th)-Pb geochronology: Which analytical capability is right for my laboratory? *Thermo Fish. Sci. Smart. Note* 30581, 2020.
- 355 Deng, X.D., Li, J.W., Luo, T., and Wang, H.Q.: Dating magmatic and hydrothermal processes using andradite-rich garnet U-Pb geochronometry, *Contrib Mineral Petr.*, 172, 71, <https://doi.org/10.1007/s00410-017-1389-2>, 2017.
- Elisha, B., Nuriel, P., Kylander-Clark, A., and Weinberger, R.: Towards in-situ U-Pb dating of dolomites, *Geochronology* 3, 337–349, <https://doi.org/10.5194/gchron-3-337-2021>, 2021.
- Evans, N.P., Turchyn, A.V., Gázquez, F., Bontognali, R.R., Chapman, H.J., and Hodell, D.A.: Coupled measurements of $\delta^{18}\text{O}$ and δD of hydration water and salinity of fluid inclusions in gypsum from the Messinian Yesares Member, Sorbas Basin (SE Spain), *Earth Planet. Sci. Lett.*, 430, 499–510, <https://doi.org/10.1016/j.epsl.2015.07.071>, 2015.
- 360 Flecker, R., and Ellam, R.M.: Identifying Late Miocene episodes of connection and isolation in the Mediterranean - Paratethyan realm using Sr isotopes, *Sediment. Geol.*, 188–189, 189–203. <https://doi.org/10.1016/j.sedgeo.2006.03.005>, 1999
- Flecker, R., Krijgsman, W., Capella, W., de Castro Martins, C., Dmitrieva, E., Mayser, J.P., Marzocchi, A., Modestu, S., Lozano, D.O., Simon, D., Tulbure, M., van den Berg, B., van der Schee, M., de Lange, G., Ellam, R., Govers, R., Gutjahr, M., Hilgen, F., Kouwenhoven, T., Lofi, J., Meijer, P., Sierro, F.J., Bachiri, N., Barhoun, N., Alami, A.C., Chacon, B., Flores, Jose A., Gregory, J., Howard, J., Lunt, D., Ochoa, M., Pancost, R., Vincent, S., and Yousfi, M.Z.: Evolution of the Late Miocene Mediterranean Atlantic gateways and their impact on regional and global environmental change, *Earth-Sci. Rev.*, 150, 365–392. <https://doi.org/10.1016/j.earscirev.2015.08.007>, 2015
- 370 Gerdes, A., and Zeh, A.: Combined U-Pb and Hf isotope LA-(MC)-ICP-MS analyses of detrital zircons: comparison with SHRIMP and new constraints for the provenance and age of an Armorican metasediment in Central Germany, *Earth Planet. Sci. Lett.*, 249, 47–61, <https://doi.org/10.1016/j.epsl.2006.06.039>, 2006.
- Gerdes, A., and Zeh, A.: Zircon formation versus zircon alteration — new insights from combined U-Pb and Lu-Hf in-situ LA-ICP-MS analyses, and consequences for the interpretation of Archean zircon from the Central Zone of the Limpopo Belt, *Chem. Geol.*, 261 (3–4), 230–243, <https://doi.org/10.1016/j.chemgeo.2008.03.005>, 2009.
- 375 Grandia, F., Asmerom, Y., Getty, S., Cardellach, E., and Canals, A.: U-Pb dating of MVT ore-stage calcite: implications for fluid flow in a Mesozoic extensional basin from Iberian Peninsula, *J. Geochem. Explor.*, 69, 377–380, [https://doi.org/10.1016/S0375-6742\(00\)00030-3](https://doi.org/10.1016/S0375-6742(00)00030-3), 2000.



- Grothe, A., Andreetto, F., Reichart, G.J., Wolthers, M., Van Baak, C.G., Vasiliev, I., Stoica, M., Sangiorgi, F., Middelburg, J.J., Davies, G.R., and Krijgsman, W.: Paratethys pacing of the Messinian Salinity Crisis: low salinity waters contributing to gypsum precipitation?, *Earth Planet. Sci. Lett.*, 532, 116029, <https://doi.org/10.1016/j.epsl.2019.116029>, 2020.
- Guillong, M., Wotzlaw, J.-F., Looser, N., and Laurent, O.: Evaluating the reliability of U-Pb laser ablation inductively coupled plasma mass spectrometry (LA-ICP-MS) carbonate geochronology: matrix issues and a potential calcite validation reference material, *Geochronology*, 2, 155-167, <https://doi.org/10.5194/gchron-2-155-2020>, 2020.
- Horstwood, M. S. A., Košler, J., Gehrels, G., Jackson, S. E., McLean, N. M., Paton, C., Pearson, N. J., Sircombe, K., Sylvester, P., Vermeesch, P., and Bowring, J. F.: Community-derived standards for LA-ICP-MS U-(Th-) Pb geochronology-Uncertainty propagation, age interpretation and data reporting, *Geostand. Geoanal. Res.*, 40, 311-332, <https://doi.org/10.1111/j.1751-908X.2016.00379.x>, 2016.
- Hsü, K.J., Ryan, W.B.F., and Cita, M.B.: Late Miocene desiccation of the Mediterranean, *Nature*, 242, 240-244, <https://doi.org/10.1038/242240a0>, 1973.
- Hsü, K. J., Montadert, L., Ross, D.A., and Neprochnov, Y.P.: Annotated record of the detailed examination of Mn deposits from DSDP Leg 42 (Holes 372 and 379A). *Pangaea*, <https://doi.org/10.1594/PANGAEA.871889>, 1978. Supplement to: Worstell, P.J., Mélières, F., Bernoulli, D., Erickson, A.J.; Wright, R., Bizon, G.; Cita, M.B., Müller, C., Kidd, R.B., Fabricius, F.H., Garrison, R.E., Hsü, K.J., and Montadert, L.: Initial Reports of the Deep Sea Drilling Project. Initial Reports of the Deep Sea Drilling Project, U.S. Government Printing Office, XLII Pt. 1, 1249 pp + 1244 pp, <https://doi.org/10.2973/dsdp.proc.42-1.1978>, 1978.
- Kameda, K., Hashimoto, Y., Wang, S.-L., Hirai, Y., and Miyahara, H.: Simultaneous and continuous stabilization of As and Pb in contaminated solution and soil by a ferrihydrite-gypsum sorbent, *J. Hazard. Mater.*, 327, 171-179, <https://doi.org/10.1016/j.jhazmat.2016.12.039>, 2017.
- Krijgsman, W., Hilgen, F. J., Raffi, I., Sierro, F. J., and Wilson, D. S.: Chronology, causes and progression of the Messinian Salinity Crisis, *Nature*, 400, 652-655, <https://doi.org/10.1038/23231>, 1999.
- Krijgsman, W., Stoica, M., Vasiliev, I., and Popov, V. V.: Rise and fall of the Paratethys Sea during the Messinian Salinity Crisis, *Earth Planet. Sci. Lett.*, 290 (1-2), 183-191, <https://doi.org/10.1016/j.epsl.2009.12.020>, 2010.
- Krijgsman, W., Capella, W., Simon, D., Hilgen, F.J., Kouwenhoven, T.J., Meijer, P.T., Sierro, F.J., Tubbare, M.A., van den Berg, B.C.J., van der Schée, M., and Flecker, R.: The Gibraltar Corridor: watergate of the Messinian Salinity Crisis, *Mar. Geol.*, 403, 238-246, <https://doi.org/10.1016/j.margeo.2018.06.008>, 2018.
- Lenoir, L., Blaise, T., Somogyi, A., Brigaud, B., Barbarand, J., Boukari, C., Nouet, J., and Pagel, M.: Uranium incorporation in fluorite and exploration of U-Pb dating, *Geochronology*, 3, 197-227, <https://doi.org/10.5194/gchron-3-199-2021>, 2021.
- Lin, J., Sun, W., Desmarais, J., Chen, N., Feng, R., Zhang, P., Li, D., Lieu, A., Tse, J.S., and Pan, Y.: Uptake and speciation of uranium in synthetic gypsum (CaSO₄·2H₂O): applications to radioactive mine tailings, *J. Environ. Radioact.*, 181, 8-17, <https://doi.org/10.1016/j.jenvrad.2017.10.010>, 2018.



- Liu, D.J., and Hendry, M.J.: Controls on ^{226}Ra during raffinate neutralization at the Key Lake uranium mill, Saskatchewan, Canada, *App. Geochem.*, 26, 2113-2120, <https://doi.org/10.1016/j.apgeochem.2011.07.009>, 2011.
- Ludwig, K.R.: User's Manual for Isoplot Version 3.75-4.15: a Geochronological Toolkit for Microsoft Excel, Berkeley
 415 Geochronological Center Special Publication, 5, 2012.
- Lugli, S., Bassetti, M.A., Manzi, V., Barbieri, M., Longinelli, A., and Roveri, M.: The Messinian 'Vena del Gesso' evaporites revisited: characterization of isotopic composition and organic matter, *J. Geol. Soc. Lond.*, 285, 179-190, <http://dx.doi.org/10.1144/SP285.11>, 2007.
- Lugli, S., Manzi, V., Roveri, M., and Schreiber, B.C.: The primary Lower Gypsum in the Mediterranean: a new facies
 420 interpretation for the first stage of the Messinian salinity crisis, *Palaeogeogr. Palaeoclimatol. Palaeoecol.*, 297, 83-99, <https://doi.org/10.1016/j.palaeo.2010.07.017>, 2010.
- Mangenot, X., Gasparrini, M., Rouchon, V. and Bonifacie, M.: Basin-scale thermal and fluid flow histories revealed by carbonate clumped isotopes ($\Delta 47$) - Middle Jurassic carbonates of the Paris Basin depocentre, *Sedimentology*, 65(1), 123-150, <https://doi.org/10.1111/sed.12427>, 2018.
- 425 Manzi, V., Gennari, R., Lugli, S., Roveri, M., and Schreiber, B.C.: The Messinian "Calcare di Base" (Sicily, Italy) revisited, *Geol. Soc. Am. Bull.*, 123, 347-370, <https://doi.org/10.1130/B30262.1>, 2011.
- Manzi, V., Gennari, R., Hilgen, F., Krijgsman, W., Lugli, S., Roveri, M., and Sierro, F.J.: Age refinement of the Messinian salinity crisis onset in the Mediterranean, *Terra Nova*, 315-322, <https://doi.org/10.1111/ter.12038>, 2013.
- Manzi, V., Gennari, R., Lugli, S., Persico, D., Reghizzi, M., Roveri, M., Schreiber, B.C., Calvo, R., Gavrieli, I., and Gvirtzman,
 430 Z.: The onset of the Messinian salinity crisis in the deep Eastern Mediterranean basin, *Terra Nova* 30 (3), 189-198, <https://doi.org/10.1111/ter.12325>, 2018.
- Meilijson, A., Hilgen, F., Sepúlveda, J., Steinberg, J., Fairbank, V., Flecker, R., Waldmann, N.D., Spaulding, S.A., Bialik, O.M., and Boudinot, F.G.: Chronology with a pinch of salt: integrated stratigraphy of Messinian evaporites in the deep Eastern Mediterranean reveals long-lasting halite deposition during Atlantic connectivity, *Earth-Sci. Rev.* 194, 374-398.
 435 <https://doi.org/10.1016/j.earscirev.2019.05.011>, 2019
- Millonig, L.J., Albert, R., Gerdes, A., Avigad, D., and Dietsch, C.: Exploring laser ablation U-Pb dating of regional metamorphic garnet - The Straits Schist, Connecticut, USA, *Earth Planet. Sci. Lett.*, 552, 116589, <https://doi.org/10.1016/j.epsl.2020.116589>, 2020.
- Montano, D., Gasparrini, M., Gerdes, A., Albert, R., Rohais, S., and Della Porta, G.: In-situ carbonate U-Pb analysis by LA-
 440 ICP-MS: From absolute dating to understanding the U-Pb partitioning in lacustrine systems, *Goldschmidt 2019 Abstracts*, 2323, 2019.
- Morales, J., Astilleros, J.M., Jiménez, A., Göttlicher, J., Steininger, R., and Fernández-Díaz, L.: Uptake of dissolved lead by anhydrite surfaces, *Appl. Geochem.*, 40, 89-96, <https://doi.org/10.1016/j.apgeochem.2013.11.002>, 2014.
- Murray, R.C.: Origin and diagenesis of gypsum and anhydrite, *J. Sedimen. Res.*, 34, 512-523,
 445 <https://doi.org/10.1306/74D710D2-2B21-11D7-8648000102C1865D>, 1964.



- Natalicchio, M., Dela Pierre, F., Lugli, S., Lowenstein, T.K., Feiner, S.J., Ferrando, S., Manzi, V., Roveri, M., and Clari, P.: Did Late Miocene (Messinian) gypsum precipitate from evaporated marine brines? Insights from the Piedmont Basin (Italy), *Geology*, 42, 179–182, <https://doi.org/10.1130/G34986.1>, 2014.
- Nuriel, P., Wotzlaw, J.F., Ovtcharova, M., Vaks, A., Stremtan, C., Šála, M., Roberts, N.M.W., and Kylander-Clark, A.R.C.:
450 The use of ASH-15 flowstone as a matrix-matched reference material for laser-ablation U – Pb geochronology of calcite, *Geochronology*, 3, 35-47, <https://doi.org/10.5194/gchron-3-35-2021>, 2021.
- Ossorio, M., Van Driessche, A.E.S., Pérez, P., and García-Ruiz, J.M.: The gypsum-anhydrite paradox revisited, *Chem. Geol.*, 386, 16-21, <https://doi.org/10.1016/j.chemgeo.2014.07.026>, 2014.
- Pagel, M., Bonifacie, M., Schneider, D. A., Gautheron, C., Brigaud, B., Calmels, D., Cros, A., Saint-Bezar, B., Landrein, P.,
455 Sutcliffe, C., and Davis, D.: Improving paleohydrological and diagenetic reconstructions in calcite veins and breccia of a sedimentary basin by combining $\Delta 47$ temperature, $\delta^{18}\text{O}$ water and U-Pb age, *Chem. Geol.*, 481, 1-17, <https://doi.org/10.1016/j.chemgeo.2017.12.026>, 2018.
- Parrish, R. R., Parrish, C. M., and Lasalle, S.: Vein calcite dating reveals Pyrenean orogen as cause of Paleogene deformation in southern England, *J. Geol. Soc.*, 175, 425-442, <https://doi.org/10.1144/jgs2017-107>, 2018.
- 460 Petrash, D.A., Bialik, O.M., Bontognali, T.R.R., Vasconcelos, C., Roberts, J.A., McKenzie, J.A., and Konhauser, K.O.: Microbially catalyzed dolomite formation: From near-surface to burial, *Earth-Sci. Rev.*, 171, 558-582, <https://doi.org/10.1016/j.earscirev.2017.06.015>, 2017.
- Piccione, G., Rasbury, E.T., Elliott, B.A., Kyle, J.R., Jaret, S.J., Acerbo, A.S., Lanzirrotti, A., Northrup, P., Wooton, K., and Parrish, R.R.: Vein fluorite U-Pb dating demonstrates post-6.2 Ma rare-earth element mobilization associated with Rio Grande
465 rifting, *Geosphere*, 15, 6, 1958- 1972, <https://doi.org/10.1130/GES02139.1>, 2019.
- Rouchy, J.M., and Caruso, A.: The Messinian salinity crisis in the Mediterranean basin: a reassessment of the data and an integrated scenario, *Sediment. Geol.*, 188–189, p. 35–67, <https://doi.org/10.1016/j.sedgeo.2006.02.005>, 2006.
- Ring, U. and Gerdes, A.: Kinematics of the Alpenrhein-Bodensee graben system in the Central Alps: Oligocene/Miocene transtension due to formation of the Western Alps arc, *Tectonics*, 35, 1367-1391, <https://doi.org/10.1002/2015TC004085>,
470 2016.
- Roberts, N. M. W., Rasbury, E. T., Parrish, R. R., Smith, C. J., Horstwood, M. S. A., and Condon, D. J.: A calcite reference material for LA-ICP-MS U-Pb geochronology, *Geochem. Geophys. Geosy.*, 18, 2807-2814, <https://doi.org/10.1002/2016GC006784>, 2017.
- Roberts, N. M. W., Drost, K., Horstwood, M. S. A., Condon, D. J., Chew, D., Drake, H., Milodowski, A. E., McLean, N. M.,
475 Smye, A. J., Walker, R. J., Haslam, R., Hodson, K., Imber, J., Beaudoin, N., and Lee, J. K.: Laser ablation inductively coupled plasma mass spectrometry (LA-ICP-MS) U-Pb carbonate geochronology: strategies, progress, and limitations, *Geochronology*, 2, 33-61, <https://doi.org/10.5194/gchron-2-33-2020>, 2020.
- Roveri, M., Lugli, S., Manzi, V., and Schreiber, B.C.: The Messinian Sicilian stratigraphy revisited: toward a new scenario for the Messinian salinity crisis, *Terra Nova*, 20, 483-488, <https://doi.org/10.1111/j.1365-3121.2008.00842.x>, 2008a.



- 480 Roveri, M., Bertini, A., Cosentino, D., Di Stefano, A., Gennari, R., Gliozzi, E., Grossi, F., Iaccarino, S.M., Lugli, S., Manzi, V., and Taviani, M.: A high-resolution stratigraphic framework for the latest Messinian events in the Mediterranean area, *Stratigraphy*, 5, 323-342, 2008b.
- Roveri, M., Flecker, R., Krijgsman, W., Lofi, J., Lugli, S., Manzi, V., Sierro, F.J., Bertini, A., Camerlenghi, A., De Lange, G., Govers, R., Hilgen, F.J., Hübscher, C., Meijer, P.T., and Stoica, M.: The Messinian Salinity Crisis: past and future of a great
485 challenge for marine sciences, *Mar. Geol.*, 352, 25-58, <https://doi.org/10.1016/j.margeo.2014.02.002>, 2014a.
- Roveri, M., Lugli, S., Manzi, V., Gennari, R., and Schreiber, B.C.: High-resolution strontium isotope stratigraphy of the Messinian deep Mediterranean basins: implications for marginal to central basins correlation, *Mar. Geol.*, 349, 113-125, <https://doi.org/10.1016/j.margeo.2014.01.002>, 2014b.
- Ryan, W.B.: Decoding the Mediterranean salinity crisis, *Sedimentology*, 56 (1), 95-136, <https://doi.org/10.1111/j.1365-3091.2008.01031.x>, 2009
490
- Schaltegger, U., Schmitt, A.K., and Horstwood, M.S.A.: U-Th-Pb zircon geochronology by ID-TIMS, SIMS, and laser ablation ICP-MS: Recipes, interpretations, and opportunities, *Chem. Geol.*, 402, 89-110, <https://doi.org/10.1016/j.chemgeo.2015.02.028>, 2015.
- Selli, R.: Il Messiniano Mayer-Eymar 1867. Proposta di un neostratotipo, *Giornale di Geologia*, 28, 1-33, 1960.
- 495 Seman, S., Stockli, D.F., and McLean, N.M.: U-Pb geochronology of grossular-andradite garnet, *Chem. Geol.*, 460, 106-116, <https://doi.org/10.1016/j.chemgeo.2017.04.020>, 2017.
- Sindern, S., Havenith, V., Gerdes, A., Meyer, F.M., Adelmann, D., and Hellmann, A.: Dating of anatase-forming diagenetic reactions in Rotliegend sandstones of the North German Basin, *Int. J. Earth Sci.*, 108, 1275-1292, <https://doi.org/10.1007/s00531-019-01705-x>, 2019.
- 500 Sylvester, P.: Matrix effects in Laser ablation-ICP-MS, in: *Laser Ablation-ICP-MS in the Earth Sciences: Current Practices and Outstanding Issues*, edited by: Sylvester, P., Mineralogical association of Canada, 67-78, 2008.
- Van Driessche, A.E.S., Stawski, T., and Kellermeier, M.: Calcium sulfate precipitation pathways in natural and engineering environments, *Chem. Geol.*, 530, 119274, <https://doi.org/10.1016/j.chemgeo.2019.119274>, 2019.
- Vasiliev, I., Mezger, E.M., Lugli, S., Reichart, G.J., Manzi, V., and Roveri, M.: How dry was the Mediterranean during the
505 Messinian salinity crisis?, *Paleogeogr. Paleoclimatol. Paleoecol.*, 471, 120-133, <https://doi.org/10.1016/j.palaeo.2017.01.032>, 2017.
- Wafforn, S., Seman, S., Kyle, J.R., Stockli, D., Leys, C., Sonbait, D., and Cloos, M.: Andradite garnet U-Pb geochronology of the big Gossan skarn, Ertzberg-Grasberg mining district, Indonesia, *Econ. Geol.*, 113, 769-778, <https://doi.org/10.5382/econgeo.2018.4569>, 2018.
- 510 Warren, J.K.: *Evaporites: A Geological Compendium*, Springer, Berlin, 1813 p, <https://doi.org/10.1007/978-3-319-13512-0>, 2016.



- Warthmann, R., van Lith, Y., Vasconcelos, C., McKenzie, J.A., and Karpoff, A.M.: Bacterially induced dolomite precipitation in anoxic culture experiments, *Geology*, 28, 1091-1094, [https://doi.org/10.1130/0091-7613\(2000\)28<1091:BIDPIA>2.0.CO;2](https://doi.org/10.1130/0091-7613(2000)28<1091:BIDPIA>2.0.CO;2), 2000.
- 515 Woodhead, J., Hellstrom, J., Maas, R., Drysdale, R., Zanchetta, G., Devine, P., and Taylor, E.: U-Pb geochronology of speleothems by MC-ICPMS, *Quat. Geochronol.*, 1, 208-221, <https://doi.org/10.1016/j.quageo.2006.08.002>, 2006.
- Woodhead, J., Hellstrom, J., Pickering, R., Drysdale, R., Paul, B., and Bajo, P.: U and Pb variability in older speleothems and strategies for their chronology, *Quat. Geochronol.*, 14, 105-113, <https://doi.org/10.1016/j.quageo.2012.02.028>, 2012.
- Yan, S., Zhou, R.J., Niu, H.C., Feng, Y.X., Nguyen, A.D., Zhao, Z.H., Yang, W.B., Qian, D., and Zhao, J.X.: LA-MC-ICP-
520 MS U-Pb dating of low-U garnets reveals multiple episodes of skarn formation in the volcanic-hosted iron mineralization system, Awulale belt, Central Asia, *GSA Bulletin*, 132 (5-6), 1031-1045, <https://doi.org/10.1130/B35214.1>, 2020
- Yang, Y.H., Wu, F.Y., Yang, J.H., Mitchell, R.H., Zhao, Z.F., Xie, L.W., Huang, C., Ma, Q., Yang, M., and Zhao, H.: U-Pb age determination of schorlomite garnet by laser ablation inductively coupled plasma mass spectrometry, *J. Anal. At. Spectrom.*, 33, 231-239, <https://doi.org/10.1039/c7ja00315c>, 2018.
- 525 Zachariasse, W.J., van Hinsbergen, D.J.J., and Fortuin, A.R.: Mass wasting and uplift on Crete and Karpathos during the early Pliocene related to initiation of south Aegean left-lateral, strike-slip tectonics, *Geol. Soc. Am. Bull.*, 120, 976-993, <https://doi.org/10.1130/B26175.1>, 2008.